Studies on the function of ebolavirus glycoprotein-specific antibodies

（エボラウイルス表面糖蛋白質に対する抗体の機能に関する研究）

Wakako FURUYAMA

Contents

Abbreviations

ADE	antibody-dependent enhancement
Alexa647-labeled Dx10	Dextran, Alexa Fluor 647, 10,000 MW
BDBV	Bundibugyo virus
BSA	bovine serum albumin
Btk	Bruton's tyrosine kinase
CT	cytoplasmic tail
CTR IgG	control IgG
DAPI	4',6-diamidino-2-phenylindole, dihydrochloride
DC-SIGN	dendritic cell-specific ICAM-3-grabbing non-integrin
DiI	1,1'-dioctadecyl-3,3,3',3'-tetramethylindocarbocyanine perchlorate
DMEM	Dulbecco's modified Eagle's medium
DMSO	Dimethyl sulfoxide
ELISA	Enzyme-linked immunosorbent assay
EBOV	Ebola virus
EVD	Ebola virus disease
FCS	fetal calf serum
FcγR	Fcγ receptor
FFU	focus forming units
GFP	green fluorescent protein
GP	glycoprotein
HEK	human embryonic kidney
hMGL	human macrophage galactose-type C-type lectin

HR1	heptad repeats 1
HR2	heptad repeats 2
IC_{50}	50% inhibitory concentrations
IFL	internal fusion loop
ITAM	immunoreceptor tyrosine-based activation motif
IU	Infectious unit
MARV	Marburg virus
MAb	monoclonal antibody
MLR	mucin-like region
NP	nucleoprotein
NPC1	Niemann-Pick C1
OD	optical density
PBS	phosphate-buffered saline
PI3K	phosphatidylinositol 3-kinase
Plat-GP	Platinum-GP
PTK	protein-tyrosine kinase
Ras	rat sarcoma
RBD	receptor binding domain
RESTV	Reston virus
RPMI	Roswell Park Memorial Institute
SDS-PAGE	sodium dodecyl sulfate-polyacrylamide gel electrophoresis
Src	sarcoma
SUDV	Sudan virus

Syk	spleen tyrosine kinase
TAFV	Taï Forest virus
TBS	Tris-buffered saline
TBST	Tris-buffered saline containing 0.1% Tween 20
TIM-1	T-cell immunoglobulin and mucin domain 1
VLP	virus-like particle
TM	transmembrane
VSV	vesicular stomatitis virus

Preface

Ebolaviruses, members of the family *Filoviridae*, cause severe hemorrhagic fever in humans and nonhuman primates, with human case fatality rates of up to 90% [1,2]. The latest epidemic of Ebola virus disease (EVD) in West Africa, ebolaviruses pose a significant public health concern. However, an effective prophylaxis or treatment for EVD is not yet commercially available. Five distinct species are known in the genus *Ebolavirus*; *Zaire ebolavirus*, *Sudan ebolavirus*, *Taï Forest ebolavirus*, *Bundibugyo ebolavirus*, and *Reston ebolavirus*, represented by Ebola virus (EBOV), Sudan virus (SUDV), Taï Forest virus (TAFV), Bundibugyo virus (BDBV), and Reston virus (RESTV), respectively [3]. In the last decade, EBOV, SUDV, and BDBV have caused EVD outbreaks with increased frequency in Central and West Africa [1,2,4].

Ebolaviruses express a single transmembrane glycoprotein (GP) that is responsible for both receptor binding and membrane fusion. GP undergoes proteolytic cleavage by host proteases such as furin, resulting in two subunits, GP1 and GP2, which are linked by a disulfide bond [5,6]. The GP1 subunit (amino acids 33-501) contains the core of the glycoprotein, a receptor binding domain (RBD), a glycan cap, and a large mucin-like region (MLR) that extends around the RBD [7]. The GP2 (amino acids 502-676) subunit contains the internal fusion loop (IFL), heptad repeats 1 and 2 (HR1 and HR2), the transmembrane region (TM), and the cytoplasmic tail (CT) [8]. EBOV entry is initiated by viral attachment to cell surface molecules such as T-cell immunoglobulin and mucin domain 1 (TIM-1) and C-type lectins [9,10], followed by internalization of the virus particle into cells via micropinocytosis [11-13]. In the late endosome, EBOV GP is cleaved by host proteases such as cathepsins L and B [14,15], and then binds to the receptor, Niemann-Pick C1 (NPC1), followed by membrane fusion [8,16-19].

Since GP is the only surface protein of ebolaviruses and essential for viral entry into host cells, it is the sole target of neutralizing antibodies. In the past, many GP-specific monoclonal antibodies (MAbs) including neutralizing antibodies, have been generated [20-23]. Previous studies have shown that neutralizing antibodies against EBOV GP reduce virus infectivity through blocking receptor binding (i.e., interaction between GP and NPC1), cathepsin proteolysis, or membrane fusion [24,25]. Importantly, passive immunization with some GP-specific MAbs protects experimental animals, such as rodents and nonhuman primates, from lethal EBOV infection [26-31]. Indeed, a human MAb cocktail against EBOV GP was used for the treatment of EVD in patients during the latest outbreak in West Africa [32-35]. However, most of the previously tested MAbs are EBOV-specific and MAb therapy against other members of the genus *Ebolavirus* (i.e., SUDV and BDBV) is not yet available.

On the other hand, some GP-specific MAbs reportedly induce antibody-dependent enhancement (ADE), a phenomenon in which viral infectivity is increased by virus-specific antibodies. ADE has been observed *in vitro* for a large number of viruses [36-38] and it has interfered with vaccinations against some viruses. In addition, some human sera convalescent from EVD contain ADE antibodies [22]. ADE of EBOV infection depends on the cross-linking of virus-antibody complexes to the cellular Fcγ receptor IIa (FcγRIIa) or complement component C1q and its ligand [22,23,39]. These receptors are known to activate various signaling pathways that lead to the reorganization of the actin cytoskeleton and membrane remodeling [40,41]. However, little is known about the molecular mechanisms underlying ADE of EBOV infection.

In this study, I describe two MAbs with different functions: neutralization and ADE. In chapter I, a broadly cross-reactive GP-specific MAb, 6D6, was generated and

analyzed for its neutralization mechanism and protective potential. In chapter II, the contribution of FcγRIIa-mediated signaling to EBOV ADE was investigated, and the function of the signaling pathway was analyzed.

Chapter I:

Discovery of an antibody for pan-ebolavirus therapy

Introduction

Several studies have demonstrated that administration of EBOV GP-specific antibodies protects nonhuman primates from lethal EBOV infection and may constitute a leading treatment option for EVD in humans [26-30]. During the West African EVD outbreak, EBOV GP-specific MAb cocktails (e.g., ZMapp) [26] were used to treat several patients [32-35]. However, most of characterized therapeutic MAbs to date are EBOV GP-specific and cross-neutralizing activity against any other ebolavirus species (e.g., SUDV and BDBV) has not been demonstrated due to antigenic differences among the species [42]. Since SUDV and BDBV have also shown their potential to cause public health emergencies during several outbreaks in Central Africa, it is difficult to determine the priority for development of countermeasure against those ebolaviruses.

In chapter I, I demonstrated generation of a broadly cross-reactive GP-specific MAb. This MAb, 6D6, recognizes the putative epitope in the highly conserved IFL and neutralizes infectivity of representative isolates of all known ebolavirus species by inhibiting the membrane fusion. I further demonstrated its protective potential as a therapeutic antibody in mouse models of EBOV and SUDV infections.

Materials and Methods

Viruses and cells. Variants Yambuku (EBOV1976), Makona (EBOV2014), Nzara (SUDV), Butalya (BDBV), Pauléoula (TAFV), Philippines89 (RESTV) and Angola (MARV), and mouse-adapted EBOV [43] were propagated in African green monkey kidney Vero E6 cells and stored at -80 ˚C. Virus titters were determined as focus forming units (FFU) by immunoplaque assays. All infectious work with filoviruses was performed in the biosafety level 4 laboratories at the Integrated Research Facility of the Rocky Mountain Laboratories, Division of Intramural Research, National Institute of Allergy and Infectious Diseases, National Institutes of Health, Hamilton, Montana, USA. Replication-competent recombinant vesicular stomatitis virus (rVSV/EBOV GP, rVSV/SUDV GP, and rVSV/RESTV GP) and replication-incompetent pseudotyped vesicular stomatitis viruses (VSVs) containing green fluorescent protein (GFP) instead of the VSV G gene were generated as described previously [20,44]. Infectious units (IUs) of replication-incompetent pseudotyped VSVs were determined using Vero E6 cells as described previously [44]. Vero E6 cells and human embryonic kidney (HEK) 293T cells were grown in Dulbecco's modified Eagle's medium (DMEM) (Sigma). The media were supplemented with fetal calf serum (FCS) (Cell Culture Bioscience) and 100 U/ml penicillin, 0.1 mg/ml streptomycin (Gibco).

Purification of virus-like particles (VLPs) for immunization. HEK293T cells were transfected with equal amounts of the expression plasmids encoding GP, matrix protein (VP40), and nucleoprotein (NP) of EBOV or SUDV using TransIT LT-1 reagent (Mirus) according to the manufacturer's instructions. Forty-eight hours later, the culture supernatant was harvested and centrifuged at 3,500 rpm for 15 min to remove cell debris.

VLPs were purified from culture supernatants by ultracentrifugation at 28,000 rpm with an SW32Ti rotor (Beckman) at 4 ˚C for 2 h with a 25% sucrose cushion. The VLP pellets were suspended in phosphate-buffered saline (PBS) and fractionated through a 20-50% sucrose gradient in PBS at 28,000 rpm with an SW41 rotor (Beckman) at 4 ˚C for 2 h. Then the VLP fractions were diluted with PBS and sedimented by ultracentrifugation at 28,000 rpm with an SW41 rotor at 4 ˚C for 2 h. Finally, the VLP pellets were resuspended in PBS.

Generation of MAb 6D6. Fifteen-week-old female BALB/c mice were immunized intraperitoneally with 100 μg of EBOV VLPs. At 2 and 5 weeks after the first immunization, the mice were intraperitoneally immunized with 100 μg of EBOV VLPs. At 10 weeks after the first immunization, the mice were immunized with 100 μg of SUDV VLPs. Two weeks after the last immunization, the mice were boosted intraperitoneally with 100 μg of EBOV VLPs. Three days later, the mice were euthanized and spleen cells and mouse myeloma P3U1 cells were fused and maintained according to a standard procedure[45]. The mice were treated daily with 75 μg/kg rapamycin intraperitoneally starting 1 week prior to the primary immunization until euthanasia. Hybridomas were screened for secretion of EBOV GP-specific MAbs by a neutralization test with VSV pseudotyped with EBOV GP and hybridomas producing MAbs were cloned twice by limiting dilution of the cells. Hybridomas producing neutralizing MAbs were further screened for the cross-reactivity to the other filovirus GPs. MAb 6D6 (IgG1) was found to be a broadly cross-neutralizing MAb and was purified from mouse ascites using protein A agarose columns (Bio-Rad). Animal studies were carried out in strict accordance with the Guidelines for Proper Conduct of Animal Experiments of the Science Council of

Japan. The protocol was approved (13-0136) by the Hokkaido University Animal Care and Use Committee.

Neutralization tests. To evaluate the neutralizing activity a focus forming assay was used. EBOV, SUDV, TAFV, BDBV, RESTV, and MARV was appropriately diluted to yield 20-100 FFUs and mixed with purified MAb 6D6 for 1 h at 37 ˚C and inoculated into confluent Vero E6 cells grown in 96-well tissue culture plates. After incubation for 3 days, the cells infected with filoviruses were fixed and stained with a mixture of anti-GP (mouse anti-EBOV GP ZGP42/3.7 or anti-MARV GP rabbit serum FS0505) and anti-NP (mouse anti-EBOV NP ZNP74/7 or anti-MARV NP rabbit serum FS0609) primary antibodies [46] followed by goat anti-mouse IgG/Alexa Fluor 488 (Invitrogen) and goat anti-rabbit IgG/Alexa Fluor 488 (Invitrogen) secondary antibodies. Virus infectivity was quantified by counting the number of fluorescent foci. VSV pseudotyped with filovirus GPs were appropriately diluted to yield 300 to 1,500 IUs and mixed with purified MAb 6D6, ZGP133/3.16, or ZGP226/8.1 for 1 h at room temperature, and inoculated into confluent Vero E6 cells grown in 96-well plates. At 20 h post-inoculation, GFP-positive cells were counted using IN Cell Analyzer 2000 (GE Healthcare). To reduce the background infectivity of the parent VSV G, pseudotyped viruses were treated with a neutralizing MAb to VSV G protein (VSV-G[N]1-9) before use. The relative percentage of infectivity was calculated by setting the number of cells infected in the absence of MAb 6D6 to 100%.

Enzyme-linked immunosorbent assay (ELISA). GP-based ELISA was performed as described previously [42]. Soluble forms of EBOV GP were purified and used as antigens.

MAbs were serially diluted with PBS containing 0.05% Tween 20 and 1% skim milk. Bound antibodies were visualized with horseradish peroxidase-conjugated goat anti-mouse IgG (H+L) (Jackson ImmunoResearch) and 3,3',5,5'-tetramethylbenzidine (Sigma). The reaction was stopped by adding 1 M phosphoric acid, and the optical density at 450 nm (OD_{450}) was measured using SoftMax Pro 6.2.1 software (Molecular Devices).

Selection of escape mutants and identification of the putative epitope. Tenfold serial dilutions of rVSV/EBOV GP, rVSV/SUDV GP, and rVSV/RESTV GP were incubated with 10 μg/ml MAb 6D6 for 1 h at room temperature and inoculated into confluent Vero E6 cells grown in 6-well tissue culture plates. After adsorption for 1 h, the cells were overlaid with Eagle's minimal essential medium (Invitrogen) containing 0.8% Bacto Agar (BD), 0.3% bovine serum albumin (BSA) (Sigma), 100 U/ml penicillin, 0.1 mg/ml streptomycin, and 10 μg/ml 6D6, and then incubated for 2 days at 37 ˚C. Mutant viruses growing in the presence of MAb 6D6 were purified from single isolated plaques at the highest dilution of the virus and propagated in Vero E6 cells. Viral RNAs were extracted from the supernatant, the nucleotide sequences of the GP genes of the parent viruses and the escape mutants were determined. The deduced amino acid sequences were compared among these viruses. The IFL amino acid sequences of EBOV, SUDV, BDBV, TAFV, RESTV, and MARV were obtained from GenBank (Accession numbers, U23187.1, U28134.1, NC_014373.1, U28006.1, AF522874.1, and KY047763, respectively). The substituted amino acid positions were mapped on the trimeric structure of GPs constructed using Discovery Studio 4.1 (Biovia) based on the crystal structure of EBOV GP (PDB code: 3CSY). The SUDV and RESTV GP structures were generated by homology modelling based on the EBOV GP structure. From 100 models of the GP trimer,

the model with the best score for probability density function (PDF) and total energy was chosen. The model was evaluated using Profiles-3D [47].

Purification and fluorescent-labeling of VLPs. For purification of VLPs, equal amounts of the expression plasmids for EBOV GP, VP40, and NP were transfected into HEK293T cells by using TransIT LT-1 (Mirus). Forty-eight hours post-transfection, the culture supernatant was harvested and centrifuged at 3,500 rpm for 15 min to remove cell debris. VLPs were precipitated through a 25% sucrose cushion by centrifugation at 11,000 rpm for 1 h at 4 ˚C with an SW32Ti rotor (Beckman). Precipitated VLPs were suspended in PBS, and fractionated through a 20-50% sucrose gradient in PBS at 27,000 rpm with an SW41 rotor (Beckman) for 2.5 h at 4 ˚C. One ml of fractionated VLPs (1 μg/ml) was incubated with 0.6 μl of 100 μM stock solution of 1,1'-dioctadecyl-3,3,3',3'-tetramethylindocarbocyanine perchlorate (DiI) (Invitrogen) in the dark for 1 h at room temperature with gentle agitation [11].

Imaging of attachment, internalization and membrane fusion of DiI-labeled VLPs. Vero E6 cells expressing enhanced GFP fused to Rab7 (eGFP-Rab7) were cultured in 35 mm glass-bottom culture dishes (MatTek Corporation). DiI-labeled VLPs were treated with 20 μg/ml 6D6 or control IgG (CTR IgG) (mouse IgG1,κ; BD Biosciences) for 1 h at room temperature. The cells were then washed with 1 ml of phenol red-free DMEM (Invitrogen) and incubated with either MAb 6D6-treated, CTR IgG-treated or untreated VLPs in the same medium on ice for 30 min. Following this, the cells were washed with the same medium to remove unbound VLPs and incubated with 200 μl of phenol red-free DMEM containing 2% FCS and 4% BSA at 37 ˚C for 0, 2, and 6 h to analyze attachment,

internalization and membrane fusion, respectively. In this assay, the fluorescent signal is enhanced once the DiI-labeled VLP envelope fuses with the endosomal membrane [11]. To count the number of DiI-labeled VLPs, the cells were fixed in 4% paraformaldehyde for 15 min at room temperature. Then nuclei were stained using 1 μg/ml of 4',6-diamidino-2-phenylindole, dihydrochloride (DAPI) for 10 min at room temperature (Thermo Fisher Scientific). Images were acquired with a 63 × oil objective lens on a Zeiss LSM700 inverted microscope and ZEN 2009 software (Carl Zeiss). For measurement of the number of DiI-labeled VLPs, images of 4-20 optical sections were acquired in 0.5-1 micron steps. The number of DiI signals was determined in approximately 100 individual cells (approximately 1-20 dots/cell) and the average number per cell was calculated for each condition. For colocalization analysis, the percentage of DiI-labeled VLPs that colocalized with eGFP-Rab7 (Both DiI- and eGFP-positive pixels/DiI-positive pixels × 100) was measured using the Coloc module in ZEN 2010 software (Carl Zeiss). The number, size, and fluorescence intensity of DiI signals were analyzed with MetaMorph software (Molecular Devices). The relative sizes and intensities of DiI signals were determined by defining the value of untreated cells as 1.

Passive immunization and protective efficacy in mice. BALB/c mice (female, 6-8 weeks old) were inoculated with mouse-adapted EBOV (1,000 FFU) by intraperitoneal injection in a total volume of 200 μl. One day after infection, the mice were treated with 100 μg of MAb 6D6 intraperitoneal in a volume of 200 μl. To investigate the potential of 6D6 to protect mice from EBOV and SUDV infection, C57BL/6 IFNAR$^{-/-}$ mice were chosen for this study as they are known to be susceptible to EBOV and SUDV infection. BDBV did not cause clinical symptoms in IFNAR$^{-/-}$ mice (data not shown). IFNAR$^{-/-}$ mice

(male and female, 5-8 weeks old) were treated with 100 μg of MAb 6D6 intraperitoneal in a volume of 200 μl one day after infection with EBOV1976 (1,000 FFU) or SUDV (1,000 FFU). The animals were monitored for signs of illness and weighed daily. Surviving mice were euthanized 28 days after infection, and serum was collected for serology. Research was approved and conducted in compliance with the guidelines of the National Institute of Allergy and Infectious Diseases/Rocky Mountain Laboratories Institutional Animal Care and Use Committee. The facility where this research was conducted is fully accredited by the Association for the Assessment and Accreditation of Laboratory Animal Care International and has an approved Office of Laboratory Animal Welfare Assurance (#A4149-01). All procedures were conducted by trained personnel under the supervision of veterinarians, and all invasive clinical procedures were performed while animals were anesthetized. Early endpoint criteria, as specified by the Institutional Animal Care and Use Committee approved scoring parameters, were used to determine when animals should be humanely euthanized.

Statistical analysis. All data were analyzed using the GraphPad Prism v6.0 software. For the viral attachment, internalization, and membrane fusion experiments, Student's *t*-test was used to evaluate differences between 6D6 and CTR IgG. To assess the weight loss of mice, I performed a 2-way repeated-measures analysis of variance (ANOVA), followed by multiple t-tests comparing the average weights of 6D6-treated and untreated (control) mice at each time point, using the Holm–Sidak method. *P* values less than 0.05 were considered to be statistically significant.

Results

***In vitro* properties of MAb 6D6**. The cross-reactive MAb 6D6 was selected by screening mouse hybridoma supernatants thoroughly for the cross-neutralizing activity of GP-specific MAbs. MAb 6D6 was found to be GP-specific and to efficiently neutralize the infectivity of VSV pseudotyped with GPs of all known ebolavirus species (EBOV, SUDV, TAFV, BDBV, and RESTV), including the variant that caused the latest outbreak in West Africa (EBOV2014), but not Marburg virus (MARV) which a related filovirus and causes human disease similar to EVD (Fig. 1A). The 50% inhibitory concentrations (IC_{50}) of 6D6 for VSVs bearing EBOV1976, EBOV2014, SUDV, TAFV, BDBV, and RESTV GPs were 0.05, 0.12, 0.19, 0.33, 0.24, and 0.62 μg/ml, respectively. I then confirmed that 6D6 effectively neutralized the infectivity of representative authentic isolates of all known ebolavirus species (Fig. 1B). Furthermore, binding experiments to EBOV GP and neutralization assays with EBOV GP-pseudotyped VSV revealed that 6D6 possessed higher binding and neutralizing abilities than EBOV GP-specific MAbs ZGP133/3.16 and ZGP226/8.1 (Fig. 1C and D), which have shown promising protective efficacy in animal models of lethal EBOV infection [28,48].

Identification of the putative 6D6 epitope. To determine the putative epitope of MAb 6D6, I utilized replication-competent recombinant VSV containing the EBOV, SUDV, or RESTV GP gene [20]. The putative epitopes of ZGP133/3.16 and ZGP226/8.1 have been successfully determined by identifying the amino acid substitutions observed in the antigenic variants escaping from neutralization by the antibodies [20,24]. I cloned 6 escape mutants of EBOV GP and found that each mutant had a single amino acid substitution, Gly-to-Arg (5/6) or Gly-to-Glu (1/6), at amino acid position 528 within the IFL sequence

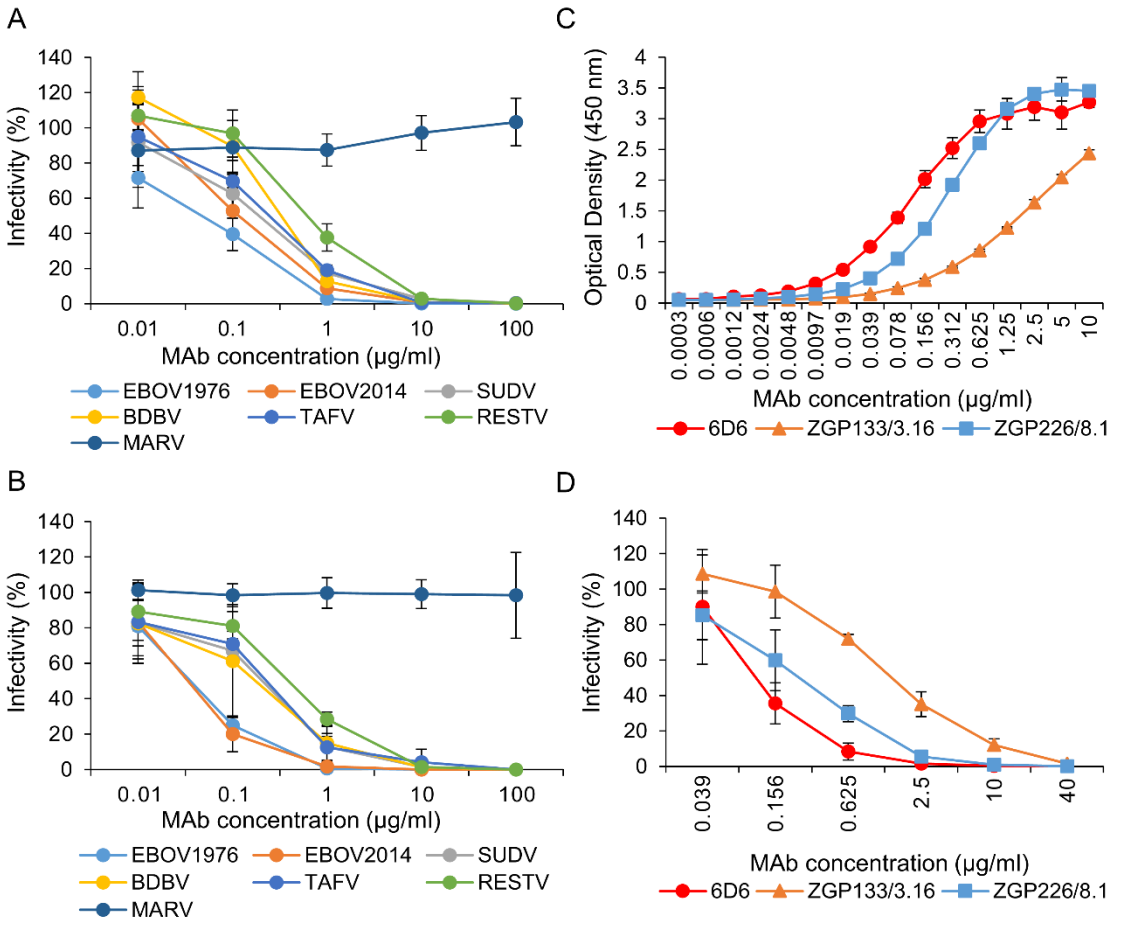

Fig. 1. Neutralizing properties of MAb 6D6 against ebolaviruses. (A) VSV pseudotyped with the indicated GPs or (B) infectious EBOV, SUDV, TAFV, BDBV, RESTV, and MARV were incubated with purified MAb 6D6 followed by inoculation into confluent Vero E6 cells. (C) Binding activities of MAbs 6D6 (red), ZGP133/3.16 (orange) and ZGP226/8.1 (blue) were examined by ELISA using EBOV GP as the antigen. (D) Neutralizing activities of MAbs 6D6 (red), ZGP133/3.16 (orange), and ZGP226/8.1 (blue) against VSV pseudotyped with EBOV GP are shown. The mean and standard deviation of three independent experiments are shown.

in the GP2 subunit (Fig. 2A). One of the six SUDV GP escape mutants had a Gly-to-Arg substitution at position 528, and other 5 SUDV GP escape mutants had an Ala-to-Thr substitution at position 530 (Fig. 2A). Two of the six RESTV GP escape mutants had a Gly-to-Glu substitution at position 529, which corresponded to position 528 of EBOV GP. A total of 3 amino acid changes were found in the other 4 RESTV GP escape mutants (Fig. 2A). Using a reverse genetics approach I verified that the Leu-to-Trp substitution at position 530 was critical for escape from 6D6 neutralization (Fig. 3). These amino acid positions, which are located at the tip of the IFL structures of EBOV, SUDV, and RESTV GPs, indicate that the loop structure including these residues is important to form the recognition site of 6D6 (Fig. 2B). I confirmed that 6D6 did not bind to the chimeric Ebola GP whose IFL region was replaced with that of MARV; however, 6D6 showed no binding activity to the synthetic peptide corresponding to the amino acids of the IFL of EBOV GP (not shown), suggesting that the 6D6 epitope may partly include other conformational structures. Importantly, the amino acid sequence of the IFL region is highly conserved among all currently known ebolaviruses (Fig. 2A), providing a novel target for universal antibody therapy against EVD caused by human-pathogenic ebolaviruses (EBOV, SUDV, TAFV, and BDBV).

Mechanism of the neutralizing activity of 6D6. Since the IFL is crucial for GP-mediated membrane fusion, I assumed that 6D6 directly inhibited the fusion step during the entry process of ebolaviruses into cells. To confirm this, I analyzed the inhibitory effects of 6D6 on viral attachment, internalization, and membrane fusion using DiI-labeled VLPs [11]. The number of 6D6-treated VLPs attached to the surface of Vero E6 cells was not significantly different from that of untreated or CTR IgG-treated VLPs, indicating that 6D6 did not

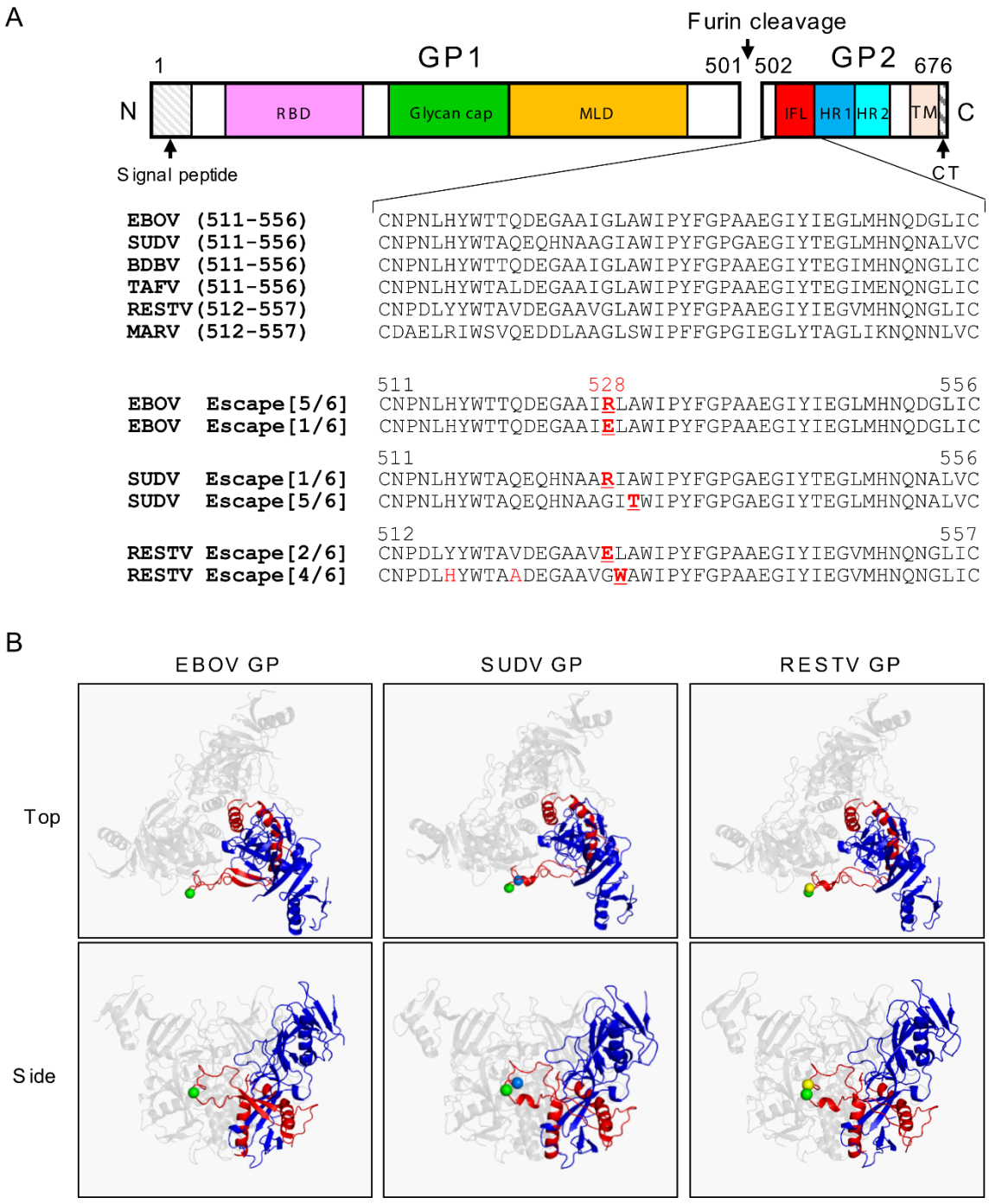

Fig. 2. Identification of the putative epitope of MAb 6D6. (A) Structure of GP and amino acid sequences of the internal fusion loop (IFL). The GP1 subunit contains the receptor binding domain (RBD), a glycan cap and a mucin-like domain (MLD). The GP2 subunit contains the IFL, heptad repeats 1 and 2 (HR1 and HR2), the transmembrane region (TM), and the cytoplasmic tail (CT). Amino acid substitutions found in the EBOV, SUDV, and RESTV GP escape mutants selected under MAb 6D6 pressure are shown in

red. (B) The amino acid residues (green, blue, and yellow spheres represent Gly, Ala, and Leu, respectively) critical for escape from the MAb 6D6 neutralization are mapped on the trimeric structure of GPs. GP1 (blue) and GP2 (red) monomers are shown as ribbon models.

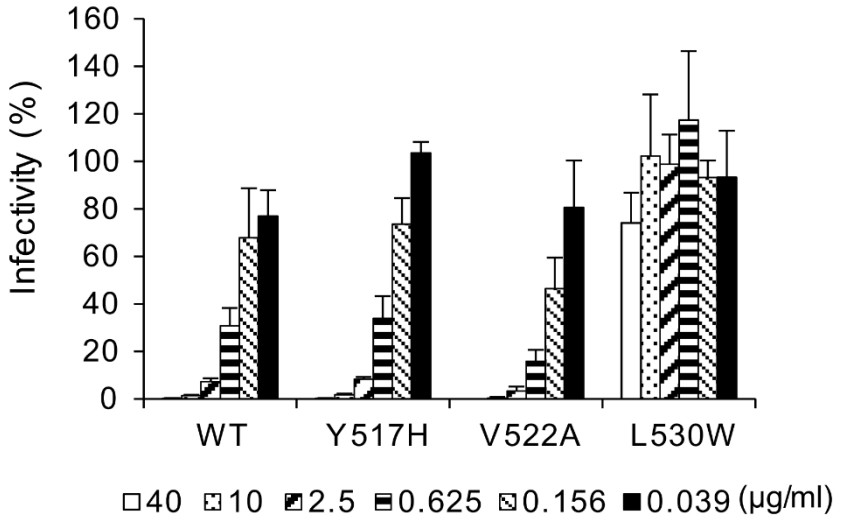

Fig. 3. Identification of the key amino acid residue on the escape mutant RESTV GP selected by MAb 6D6. Two RESTV GP mutants had the same Gly-to-Glu substitution at position 529, which is the corresponding position of the EBOV GP mutants, whereas three amino acid changes were found in the other 4 mutants of RESTV GP: Tyr at position 517, Val at position 522, and Leu at position 530 were replaced with His, Ala, and Trp, respectively (Fig. 2B). To clarify which amino acid change was critical for escaping from the 6D6 neutralization, I generated RESTV GP mutants with single amino acid substitutions for each position (Y517H, V522A, and L530W), and investigated the neutralizing activity of MAb 6D6 against VSV pseudotyped with these single amino acid mutants of RESTV GP. The mean and standard deviation of three independent experiments are shown.

interfere with VLP attachment (Fig. 4A and D). Likewise, the number of VLPs that colocalized with eGFP-Rab7, a late endosome marker, was similar, suggesting that 6D6 did not affect subsequent uptake into cells (Fig. 4B and E). Finally, I analyzed membrane fusion efficiency by detecting dequenched DiI fluorescence [11,46]. I observed remarkably enlarged and enhanced DiI signals colocalizing with Rab7 in cells incubated with untreated and CTR IgG-treated VLPs, indicating that membrane fusion occurred efficiently in the endosomes (Fig. 4C left and middle panels). In contrast, the size and intensity of DiI signals from 6D6-treated VLPs were significantly reduced, indicating that 6D6 prevented GP-mediated membrane fusion (Fig. 4C right panels and F).

Protective efficacy of MAb 6D6 in mouse models. Finally, I investigated the potential of 6D6 to protect mice from ebolavirus infections (Fig. 5). Immunocompetent BALB/c mice were infected with a lethal dose of mouse-adapted EBOV and treated 24 h later with 100 μg of 6D6. The treated animals survived without clinical symptoms, whereas untreated mice succumbed to infection within 9 days (Fig. 5A). I further evaluated the cross-protective potential of 6D6 against wild-type EBOV and SUDV infections (Fig. 5B). Since immunocompetent mice do not develop disease upon infection with these wild-type ebolavirus isolates, interferon α/β receptor knockout ($IFNAR^{-/-}$) C57BL/6 mice were used for this purpose. I found that both EBOV and SUDV caused severe weight loss in untreated mice, whereas only EBOV uniformly caused a lethal infection. Treatment with 6D6 24 h after infection delayed the onset of the disease caused by these ebolaviruses and significantly reduced the weight loss in this immunocompromised mouse strain. All 6D6-treated mice survived the EBOV infection.

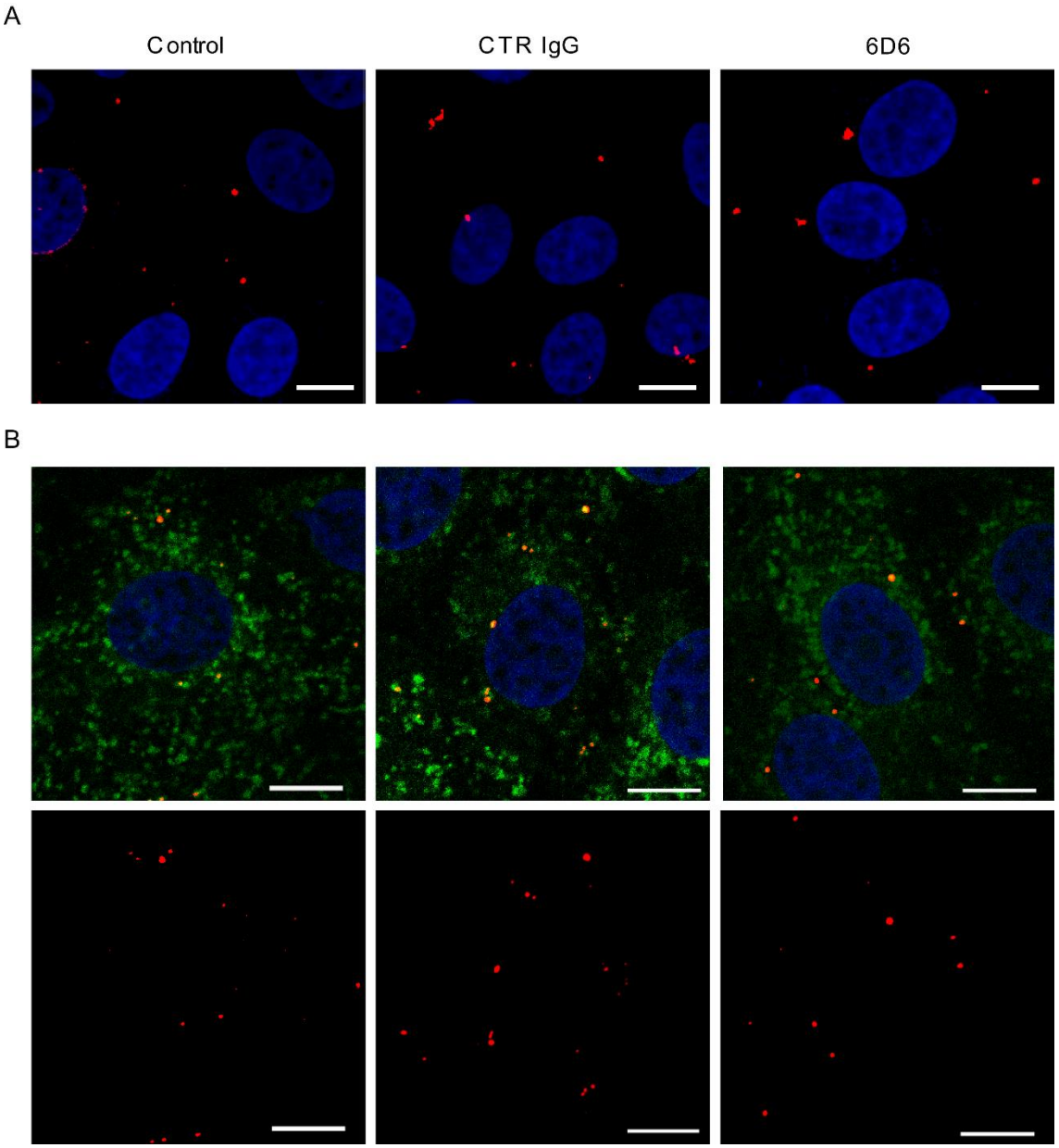
A
Control
CTR IgG
6D6
B

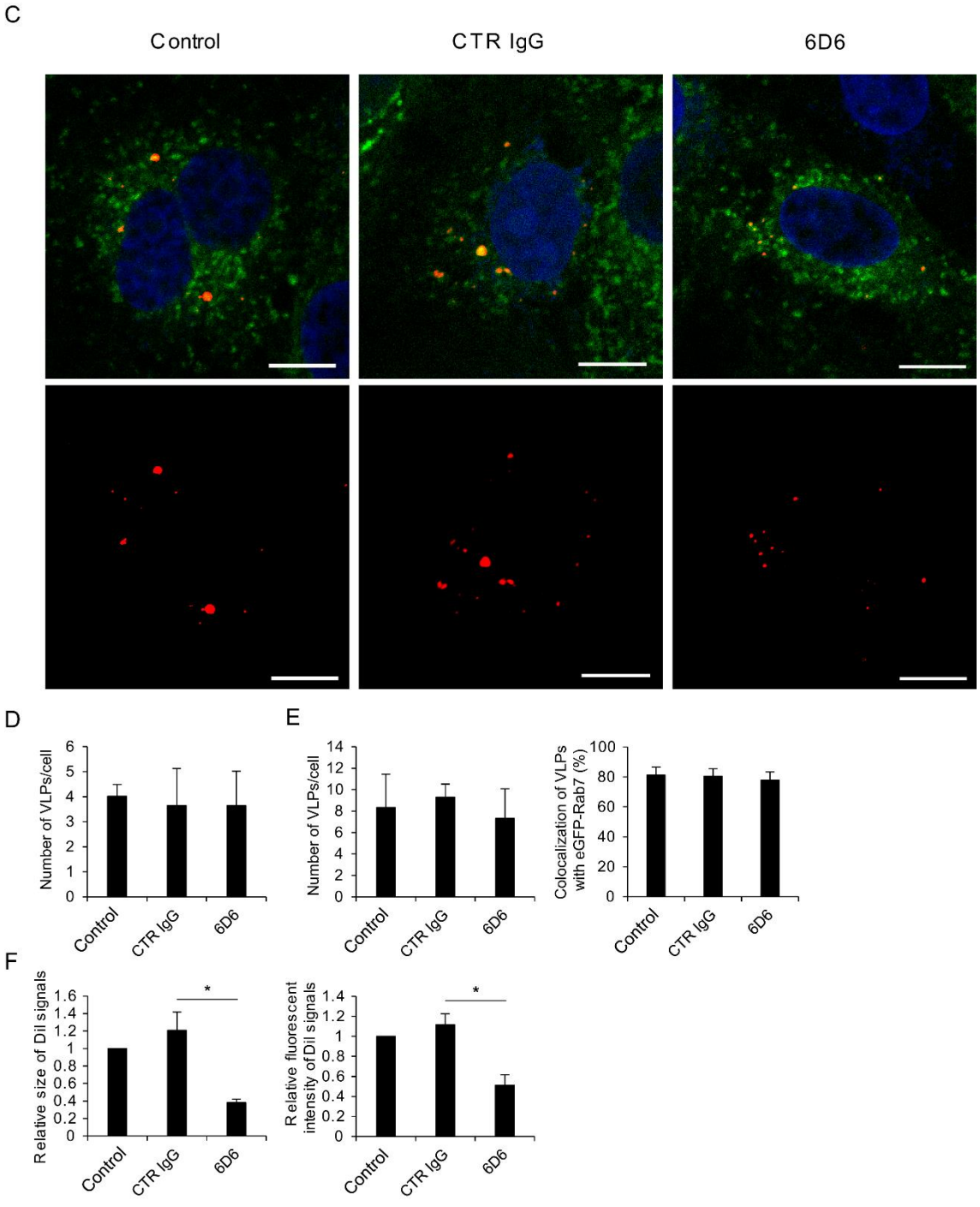

Fig. 4. Effect of MAb 6D6 on virus entry. (A-C) Fluorescent images of attachment and internalization of VLP. (D-F) Quantified fluorescent signals of VLP and Rab7. Untreated (Control), CTR IgG (CTR IgG)- or 6D6-treated DiI-labeled VLPs were inoculated into confluent Vero E6 cells expressing eGFP-Rab7 and incubated for 30 min on ice. After adsorption, the cells were incubated for 0 (A and D), 2 (B and E) and 6 h (C and F) at 37 ˚C. DiI signals on the cell surface (A) and in the cytoplasm (B and C) were monitored by

confocal laser scanning microscopy. The number, size, and fluorescence intensity of DiI signals were quantified. Scale bars represent 10 μm. The means and standard deviations of three independent experiments are shown. Statistical analysis was performed using Student's *t*-test (*p<0.05).

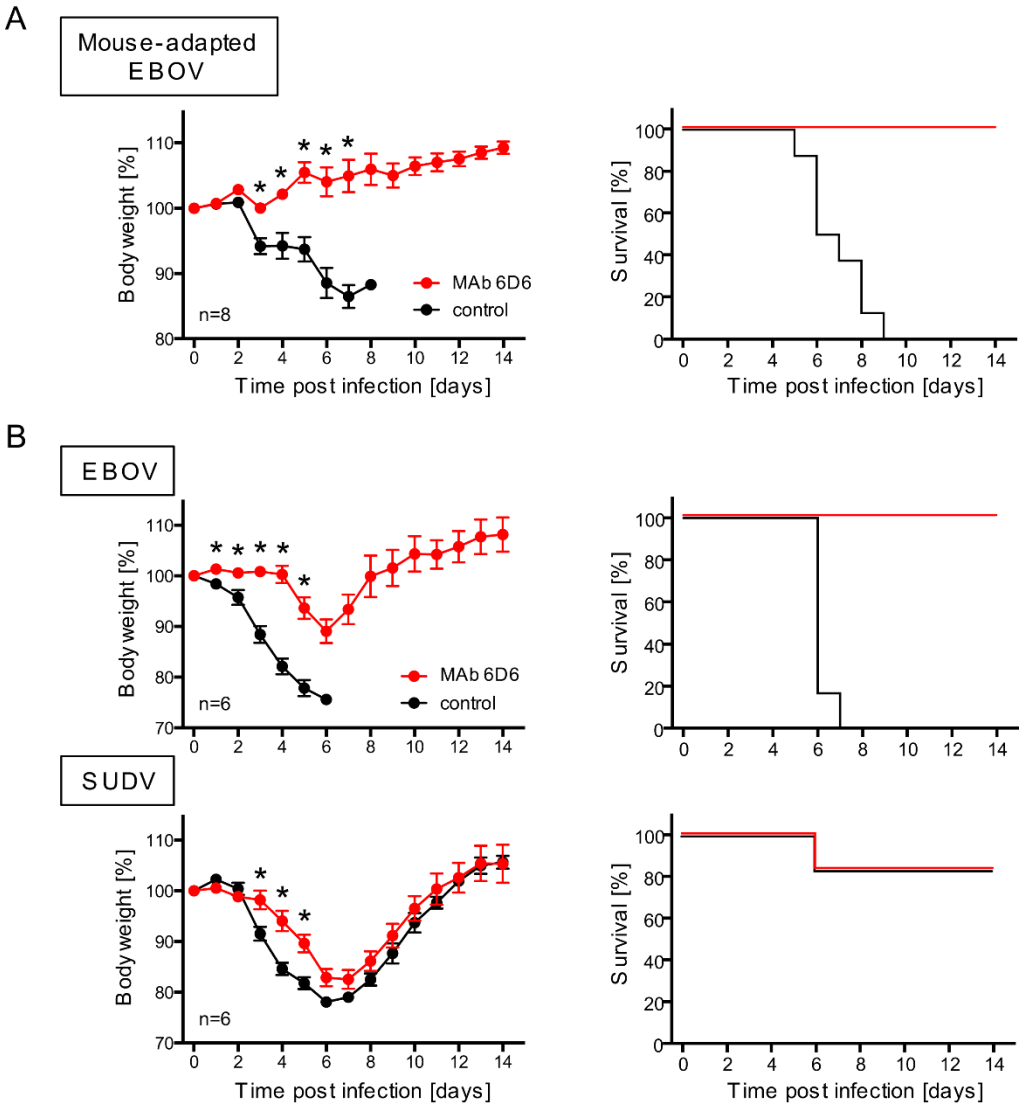

Fig. 5. Protective efficacy of MAb 6D6 in mice. (A) BALB/c mice (n = 8) were intraperitoneally infected with a lethal dose of mouse-adapted EBOV. (B) IFNAR$^{-/-}$ mice (n = 6) were intraperitoneally infected with EBOV1976 (upper panels) or SUDV (bottom panels). Twenty-four hours after infection, animals were treated intraperitoneally with either 100 µg of MAb 6D6 or a vehicle control (PBS). The animals were then monitored for 14 days for clinical signs of infection and weighed daily. Body weight (left panels) and survival curves (right panels) are shown. Error bars indicate standard error of the mean. Significant differences are indicated by asterisks (*p<0.05).

Discussion

Neutralizing antibody-based therapies have been tested in animal models and clinical trials with particular attention given to highly lethal viral diseases [49]. Passive immunization with convalescent serum has also been tested for EBOV-infected patients [50,51]. Recent studies have demonstrated the effectiveness of MAb treatments in nonhuman primate models of EVD [26,28-30,52,53], and GP-specific MAb cocktails, ZMapp and ZMAb, were used in clinical cases during the 2014 EVD outbreak caused by EBOV (belonging to *Zaire ebolavirus*) [32-35]. However, these MAb cocktails are not expected to be cross-protective against the other antigenically distinct ebolaviruses. On the other hand, highly cross-reactive MAbs against all known ebolaviruses have been generated previously, but none of those has neutralizing activity [42,54]. In this study, I generated the novel MAb 6D6, which has cross-neutralizing activity against all known ebolaviruses.

I showed that 6D6 reduced infectivities of all known ebolaviruses *in vitro* with higher neutralizing and binding activities than the EBOV GP-specific MAbs ZGP133/3.16 and ZGP226/8.1. Indeed, the IC_{50} values of 6D6 were equal to or lower than those of previously reported neutralizing MAbs [55-57], suggesting its protective capacity as a therapuetic MAb. By analyzing the amino acid substitution observed in the antigenic variants escaping from 6D6, I determined the putative epitope of 6D6 in the IFL on the GP molecule, which may overlap that of a partially cross-reactive GP-specific MAb reported recently [58]. Accordingly, 6D6 directly inhibited the membrane fusion induced by EBOV VLPs in endosomes/lysosomes. The IFL structure is highly conserved in all species of ebolaviruses, indicating that this region can be targeted for both vaccine and therapeutic development against ebolaviruses. Since the putative epitope of 6D6 is different from those previously reported for other GP-specific MAbs used in passive

immunization studies [20,56,59-62]. 6D6 may provide a promising option as a component of antibody cocktails in combination with other previously tested MAbs.

I further demonstrated that passive immunization with 6D6 protected both BALB/c and IFNAR$^{-/-}$ C57BL/6 mice from lethal infection by EBOV (i.e., mouse-adapted and wild-type EBOV, respectively). However, the cross-protective potential of 6D6 could only be evaluated for disease severity using IFNAR$^{-/-}$ C57BL/6 mice since mouse-adapted SUDV causing lethal infection in immunocompetent mice is not currently available and SUDV did not uniformly cause lethal infection even in this immunocompromised mouse strain. I found that passive immunization with 6D6 significantly reduced the weight loss in SUDV-infected mice, although the extent was not as prominent as in EBOV-infected mice. The less significant protective effects seen in SUDV-infected mice might have been due to the higher IC_{50} value of 6D6 against SUDV than against EBOV. Thus, these results supported the *in vitro* characteristics of 6D6 and demonstrated the effectiveness of the 6D6 treatment *in vivo* against multiple species of ebolaviruses. A previous study demonstrated that immunocompromised mice treated several times with 500 μg of MAb SUDV-specific MAbs were protected from SUDV infection [63], whereas mice were treated once with 100 μg of 6D6 in this study. Thus, I assume that the protective effect against SUDV could be improved by increased doses of 6D6.

The broadly cross-neutralizing antibody 6D6 recognizing the common epitope shared among all currently known ebolaviruses, converted into a human-mouse chimeric MAb [28], is a promising therapeutic candidate. On the other hand, the generation of 6D6 escape mutants *in vitro* speaks against monotherapy with this MAb and may favor the development of antibody cocktails including 6D6 for future pan-ebolavirus therapy. For

other viruses, it has indeed been reported that combination of MAbs helps to avoid the appearance of escape variants if these MAbs recognize distinct epitopes [64-66]. While the detailed mechanisms underlying antibody-mediated protection from ebolavirus infection need to be further elucidated, the discovery of this highly cross-reactive neutralizing antibody and its putative epitope reported here provides a promising option for the development of a universal EVD therapy and will accelerate the design and implementation of improved therapeutics and vaccines that can selectively elicit cross-neutralizing antibodies against multiple species of ebolaviruses.

Summary

During the latest outbreak of EVD in West Africa, MAb therapy (e.g., ZMapp) was utilized to treat patients. However, due to the antigenic differences among the five ebolavirus species, the current therapeutic MAbs are only effective against viruses of the species *Zaire ebolavirus*. Although this particular species has indeed caused the majority of human infections in Central and, recently, West Africa, other ebolavirus species (e.g., *Sudan ebolavirus* and *Bundibugyo ebolavirus*) have also repeatedly caused outbreaks in Central Africa and thus should not be neglected in the development of countermeasures against other ebolavirus species. Here I report the generation of an ebolavirus GP-specific MAb that effectively inhibits cellular entry of representative isolates of all known ebolavirus species *in vitro* and show its protective efficacy in mouse models of ebolavirus infections. This novel neutralizing MAb targets a highly conserved IFL in the GP molecule and prevents membrane fusion of the viral envelope with cellular membranes. The discovery of this highly cross-neutralizing antibody provides a promising option for broad-acting ebolavirus antibody therapy and will accelerate the design of improved vaccines that can selectively elicit cross-neutralizing antibodies against multiple species of ebolaviruses.

Chapter II:

Fcγ-receptor IIa-mediated Src signaling pathway is essential for the antibody-dependent enhancement of Ebola virus infection

Introduction

It has been demonstrated that EBOV exploits some GP-specific antibodies for its entry into cells, leading to increased infectivity *in vitro* [22,39]. This phenomenon has been described for a number of viruses and is known as ADE [36-38]. For some of these viruses, ADE has become a great concern to disease control by vaccination. Particularly, convalescent human sera have been shown to contain ADE antibodies [22,39], raising concerns about potential detrimental effects of passive immunization with convalescent human sera, which is currently under consideration for treatment of EVD. Two distinct pathways of EBOV ADE, one mediated by Fc receptors and the other by complement component C1q and its ligands, are known [22,23]. In particular, the FcγR is commonly involved in ADE of virus infections [67,68]. However, the molecular mechanisms underlying ADE-mediated virus entry through FcγR are not fully understood.

Three classes of FcγR, FcγRI (CD64), FcγRII (CD32), and FcγRIII (CD16), are expressed in various human immune cells such as dendritic cells, monocytes, and B lymphocytes [69]. Among these FcγRs, FcγRII is a key molecule for EBOV ADE of infection in human leukemia K562 cells [23]. Human FcγRII exists in two isoforms, FcγRIIa and FcγRIIb, which differ in their signal peptides and cytoplasmic tails. FcγRIIa is the active form of FcγRII and contains an immunoreceptor tyrosine-based activation motif (ITAM) in its cytoplasmic tail [69]. The cytoplasmic tail of FcγRIIa is known to contribute to the activitation of two structurally and functionally distinct protein-tyrosine kinase

(PTK) classes, the sarcoma (Src) family PTKs [70,71] and spleen tyrosine kinase (Syk) [72]. In addition, Syk is reported to participate in activation of enzymes such as rat sarcoma (Ras), phosphatidylinositol 3-kinase (PI3K), and Bruton's tyrosine kinase (Btk) [69,73]. These signaling pathways are known to be important for the induction of phagocytic and endocytic processes to internalize immune complexes [69,73,74].

In the chapter II, I focused on the role of FcγRIIa and investigated the contribution of FcγRIIa-mediated signaling to the ADE of EBOV infection. I show that Src family PTKs are essential for EBOV ADE-mediated entry. My data indicate that binding of antibody-virus complexes to the cell surface FcγRIIa triggers phosphorylation of Src family PTKs and activates subsequent signaling pathways, leading to enhanced viral uptake through phagocytosis and/or macropinocytosis.

Materials and Methods

Viruses and cells. EBOV expressing GFP [75] was propagated in Vero E6 cells and stored at -80 ˚C. Replication-incompetent VSV pseudotyped with EBOV GP containing GFP instead of the VSV G gene (VSV-EBOV GP) was generated as described previously [20,44]. Virus titers were determined as IUs by counting GFP-positive cells. All infectious work with EBOV was performed in the biosafety level 4 laboratory at the Integrated Research Facility of the Rocky Mountain Laboratories, Division of Intramural Research, National Institute of Allergy and Infectious Diseases, National Institutes of Health, Hamilton, Montana, USA. Vero E6 cells and HEK 293T cells were grown in DMEM (Sigma), and human chronic myelogenous leukemia K562 cell line and K562 cell lines stably expressing dendritic cell-specific ICAM-3-grabbing non-integrin (DC-SIGN) or human macrophage galactose-type C-type lectin (hMGL) [76,77] and human leukemic Jurkat T cells were grown in Roswell Park Memorial Institute (RPMI) 1640 medium (Sigma). These media were supplemented with 10% FCS (Cell Culture Bioscience), 100 U/ml penicillin, and 0.1 mg/ml streptomycin (Gibco).

Generation of FcγRIIa- or FcγRIIaΔCT-expressing Jurkat T cells. The FcγRIIa gene was PCR-amplified from a full-length cDNA library prepared from K562 cells using the primers, EcoRI-FcγRIIa (5'-GGGAATTCGGATGACTATGGAGACCCAA-3') and FcγRIIa-XhoI (5'-ATTTCTCGAGTTTGTCATCCACTCAGCAAG-3'). Mutant FcγRIIa lacking its cytoplasmic tail (amino acid positions 241-317) (FcγRIIaΔCT) was generated using a PrimeSTAR Mutagenesis Basal Kit (Takara). After sequence confirmation, these PCR products were cloned into a murine leukemia virus-based retroviral vector, pMXs-Puro Retroviral Vector (Cell Biolabs). To generate the retrovirus, 293T-derived Platinum-

GP (Plat-GP) cells (Cell Biolabs) were cotransfected with pMXs-puro encoding FcγRIIa or FcγRIIaΔCT and the expression plasmid pCAGGS encoding the VSV G protein using Lipofectamine 2000 (Invitrogen). Forty-eight h later, the culture supernatants containing retroviruses were collected, clarified through 0.45 μm filters, and then used to infect Jurkat T cells. Jurkat T cell lines stably expressing FcγRIIa or FcγRIIaΔCT were selected with RPMI medium containing 10% FCS, 100 U/ml penicillin, 0.1 mg/ml streptomycin, and 10 μg/ml puromycin (Sigma-Aldrich). For some experiments, each Jurkat T cell line was cloned by limiting dilution to enrich the population of FcγRIIa-expressing cells. To check the expression levels of FcγRIIa and FcγRIIaΔCT, these cells were incubated with a mouse anti-CD32 monoclonal antibody (GeneTex) for 1 h at room temperature. After washing 3 times with PBS, binding of the primary antibody was detected with Alexa647-conjugated F(ab')2-goat anti-mouse IgG (H+L) (Jackson ImmunoResearch). After further washing 3 times with PBS, the fluorescent intensity of the cells was analyzed using a FACS Canto flow cytometer (BD Biosciences) and FlowJo software (Tree Star).

ADE assays. EBOV was appropriately diluted to yield 50-100 IUs in K562 cells and then incubated for 30 min-1 h at 37 ˚C with or without 10 μg/ml MAbs. The anti-EBOV GP MAb ZGP12/1.1 (IgG2a), which is known to enhance EBOV infection *in vitro*, was used as the ADE MAb [39]. S139/1 (IgG2a), a MAb specific to influenza A virus hemagglutinin, was used as the control IgG (CTR IgG) [78]. K562 and Jurkat T cells were inoculated with EBOV alone or EBOV/MAb mixtures and incubated for 72 h. Virus infectivity was measured by counting the number of GFP-positive cells in FACS and analyzed using FlowJo software. VSV-EBOV GP was appropriately diluted to yield 50-100 IUs in K562 cells and incubated for 1 h at room temperature with or without 1 μg/ml MAbs, and then

inoculated into K562 and Jurkat T cells. Twenty-four h later, GFP-positive cells were counted using an IN Cell Analyzer 2000 (GE Healthcare). To reduce the background (i.e., residual) infectivity of the parent VSV, VSV-EBOV GP was treated with a neutralizing MAb to VSV G protein (VSV-G[N]1-9) before use.

Purification and DiI-labeling of VLPs. For purification of VLPs, HEK293T cells were transfected with equal amounts of the expression plasmids encoding EBOV or SUDV GP, VP40, and NP using TransIT LT-1 (Mirus) according to the manufacturer's instructions. Forty-eight h after transfection, the culture supernatant was harvested and centrifuged at 3,500 rpm for 15 min at 4 ˚C to remove cell debris. VLPs were precipitated through a 25% sucrose cushion by centrifugation at 11,000 rpm for 1 h at 4 ˚C with an SW32Ti rotor (Beckman). Pelleted VLPs were suspended in PBS, and fractionated through a 20-50% sucrose gradient in PBS at 28,000 rpm with an SW41 rotor (Beckman) for 2 h at 4 ˚C. One ml of 1 μg/ml fractionated VLPs was incubated with 0.6 μl of 100 μM DiI (Molecular Probes) in the dark for 1 h at room temperature with gentle agitation [11].

Imaging of attachment and internalization of DiI-labeled VLPs. The eGFP-Rab7 fusion protein gene was cloned into a Moloney murine leukemia virus-based retrovirus plasmid [11,79], and recombinant retroviruses for the expression of eGFP-Rab7 were produced and used to infect K562 cells as described above. K562 and Jurkat T cell lines were cultured in 35 mm glass-bottom dishes (MatTek Corporation) precoated with borate buffer containing 0.1 mg/ml poly-L-lysine (Sigma). The cells were washed with phenol red-free RPMI (Gibco) and inoculated with 100 μl of 1 μg/ml DiI-labeled VLPs treated with 20 μg/ml ZGP12/1.1 or CTR IgG for 1 h at room temperature, followed by

incubation for 30 min on ice. They were then washed twice with the same medium to remove unbound DiI-labeled VLPs and incubated with phenol red-free RPMI containing 2% FCS and 4% BSA for 0 and 2 h at 37 ˚C to analyze DiI-labeled VLP attachment and internalization, respectively. To count the number of DiI-labeled VLPs, the cells were fixed with 4% paraformaldehyde for 15 min at room temperature. Then the nuclei were stained with 1 μg/ml DAPI (Molecular Probes) for 10 min at room temperature. Microscopic images were acquired with a 63 × oil objective lens on a Zeiss LSM780 inverted microscope and ZEN 2010 software (Carl Zeiss). For measurement of the number of DiI-labeled VLPs, images of 4-20 optical sections were acquired in 1 micron steps. The number of DiI-labeled VLPs was determined in approximately 100 individual cells using MetaMorph software (Molecular Devices) and the average number per cell was calculated for each condition. For colocalization analysis, the percentage of DiI-labeled VLPs that colocalized with eGFP-Rab7 (Both DiI- and eGFP-positive pixels/DiI-positive pixels × 100) was measured in approximately 100 individual cells using the Coloc module in ZEN 2010 software (Carl Zeiss).

Dextran uptake assays. One μg/ml DiI-labeled VLPs were treated with 20 μg/ml CTR IgG or ZGP12/1.1 for 1 h at room temperature. K562 and Jurkat T cell lines were cultured in poly-L-lysine-coated glass-bottom culture dishes and incubated with 100 μl untreated, CTR IgG-, or ZGP12/1.1-treated DiI-labeled VLPs for 30 min on ice. The cells were washed twice with phenol red-free RPMI and then incubated with phenol red-free RPMI containing 2% FCS, 4% BSA, and 0.5 mg/ml Dextran, Alexa Fluor 647, 10,000 MW (Alexa647-labeled Dx10) (Molecular Probes) for 1-2 h at 37 ˚C. After washing twice with phenol red-free RPMI to remove surface-unbound DiI-labeled VLPs and Alexa647-

labeled Dx10, and the cells were fixed with 4% paraformaldehyde for 15 min at room temperature. Then, the nuclei were stained with 1 μg/ml DAPI for 10 min at room temperature. Internalized DiI-labeled VLPs and Alexa647-labeled Dx10 were analyzed by confocal laser scanning microscopy as described above. The percentage of DiI-labeled VLPs that colocalized with Alexa647-labeled Dx10 (Both DiI- and Alexa647-positive pixels/DiI-positive pixels × 100) was measured in approximately 100 individual cells using the Coloc module in ZEN 2010 software. The number and size of Dx10-positive vesicles were analyzed with MetaMorph software.

Inhibitor treatments. For infection assays, the Syk inhibitor R788 (Santa Cruz), Src family PTK inhibitor PP2 (Tocris), BTK inhibitor LFM-A13 (Focus Biomolecules), PI3K inhibitor LY294002 (Wako), and Ras inhibitor Manumycin A (Santa Cruz) were used for treatments of K562 cells. R788, LFM-A13, and LY294002 were used at 0.15-40 μM. PP2 and Manumycin A were used at 0.15-10 μM. For imaging analysis, K562 cell lines were cultured in 35 mm glass-bottom dishes precoated with poly-L-lysine, and then treated with 20 μM PP2 for 1 h at 37 ˚C. PP2-treated cells were washed with phenol red-free RPMI and inoculated with untreated, CTR IgG-, or ZGP12/1.1-treated DiI-labeled VLPs for 30 min on ice in the presence of 20 μM PP2 in the same medium. The cells were then washed twice with the same medium and incubated with phenol red-free RPMI containing 2% FCS, 4% BSA, and 20 μM PP2 for 0 and 2 h at 37 ˚C. Then they were fixed and analyzed by confocal laser scanning microscopy as described above. Dimethyl sulfoxide (DMSO, Sigma-Aldrich) or ethanol (Kanto Chemical) was used as a solvent control.

Generation of Src or Syk knockdown K562 cells. Plat-GP cells were cotransfected with

pRS (retroviral plasmids) encoding human Src or Syk shRNA (ORIGENE) and the expression plasmid pCAGGS encoding the VSV G protein using Lipofectamine 2000 (Invitrogen). ShSrc target sequences were: shSrc1:5'-GGAGGCTTCAACTCCTCGGACACCGTCAC-3', shSrc2: 5'-AAGAAAGGCGAGCGGCTCCAGATTGTCAA-3', shSrc3: 5'-GCAGTTGTATGCTGTGGTTTCAGAGGAGC-3', shSrc4: 5'-CTGGAGGCAATCAAGCAGACATAGAAGAG-3'. ShSyk target sequences were: shSyk1:5'- GAATATGTGAAGCAGACATGGAACCTGCA-3', shSyk2: 5'-GGAGGAGGCAGAAGATTACCTGGTCCAGG-3', shSyk3: 5'-TGTCATTCAATCCGTATGAGCCAGAACTT-3', shSyk4: 5'-CTCTGGCAGCTAGTCGAGCATTATTCTTA-3'. After incubation for 48 h, culture supernatants containing the retroviruses expressing human Src or Syk shRNAs were collected, clarified through 0.45-μm filters, and then used to infect K562 cells. Transduced K562 cell lines were selected with RPMI medium containing 10% FCS, 100 U/ml penicillin, 0.1 mg/ml streptomycin, and 5 μg/ml puromycin (Sigma-Aldrich). To check the knockdown efficiency for Src and Syk, cells were collected and washed once with PBS and treated with lysis buffer (0.1% Nonidet P-40, 150 mM NaCl, 1 mM EDTA, 10 mM Tris HCl, pH 7.8) in the presence of a protease inhibitor cocktail, Complete mini (Roche). Then the lysates were mixed with sodium dodecyl sulfate-polyacrylamide gel electrophoresis (SDS-PAGE) sample buffer (Bio-Rad) with 5% 2-mercaptoethanol (Wako) and boiled for 5 min. The samples were electrophoresed by SDS-PAGE on 5 to 20% gradient polyacrylamide gel, SuperSep Ace (Wako), and separated proteins were blotted on a polyvinylidene difluoride membrane (Millipore). The membrane was blocked for at least 1 h at room temperature with Tris-buffered saline containing 0.1%

Tween 20 (TBST) and 1% BSA. Then the membrane was incubated with a rabbit anti-Src antibody (36D10: Cell Signaling) or mouse anti-Syk antibody (4D10.1: Abcam) in TBST containing 1% BSA, followed by incubation with horseradish peroxidase-conjugated donkey anti-rabbit IgG (H+L) or horseradish peroxidase-conjugated goat anti-mouse IgG (H+L) (Jackson ImmunoResearch), respectively, and visualization by Immobilon Western (Millipore). Band intensities were analyzed with a VersaDoc Imaging System (Bio-Rad) and quantified with Image Lab version 3.0 software (Bio-Rad).

Phosphorylation assay. One μg/ml purified VLPs were treated with 20 μg/ml ZGP12/1.1 or CTR IgG for 1 h at room temperature. K562 cells were incubated with DMSO or 20 μM PP2 for 1 h at 37 ˚C. Untreated or PP2-treated K562 cells were inoculated with untreated, CTR IgG-, or ZGP12/1.1-treated VLPs and incubated for 0, 10, 30, or 60 min at 37 ˚C. At each time point, cells were collected and washed once in PBS and treated with lysis buffer (0.1% Nonidet P-40, 150 mM NaCl, 1 mM EDTA, 10 mM Tris HCl, pH 7.8) in the presence of a protease inhibitor cocktail, Complete mini (Roche), and a phosphatase inhibitor cocktail, PhosSTOP (Roche). Then the lysates were mixed with SDS-PAGE sample buffer (Bio-Rad) with 5% 2-mercaptoethanol (Wako) and boiled for 5 min. The samples were electrophoresed by SDS-PAGE on 5 to 20% gradient polyacrylamide gel, SuperSep Ace (Wako), and separated proteins were blotted on a polyvinylidene difluoride membrane (Millipore). The membrane was blocked for at least 1 h at room temperature with TBST and 1% BSA. Then the membrane was incubated with a rabbit anti-phospho-Src family (Tyr416) antibody (Cell Signaling) in TBST containing 1% BSA, followed by visualization using horseradish peroxidase-conjugated donkey anti-rabbit IgG (H+L) (Jackson ImmunoResearch) and Immobilon Western

(Millipore). Band intensities were analyzed with a VersaDoc Imaging System (Bio-Rad) and quantified with Image Lab version 3.0 software (Bio-Rad).

Statistical analysis. All data were analyzed using Excel software. In all experiments, Student's *t*-test was used to evaluate statistical differences. *P* values of less than 0.05 were considered to be significant.

Results

Cytoplasmic tail of FcγRIIa is required for ADE of EBOV infection. To investigate the role of FcγRIIa and, in particular, the importance of its cytoplasmic tail in EBOV ADE, I compared the functions of wild-type FcγRIIa and FcγRIIaΔCT which is a deletion mutant of FcγRIIa lacking its cytoplasmic tail. Both molecules were expressed on Jurkat T cells, which are known to be poorly permissive for EBOV infection [80] and lack this Fc receptor [81]. Jurkat T cells were transduced with full-length FcγRIIa or FcγRIIaΔCT genes using a retrovirus vector (Fig. 6A and B) and subsequently infected with VSV-EBOV GP and infectious EBOV in the presence or absence of the GP-specific MAb ZGP12/1.1, which is known to induce EBOV ADE [39] (Fig. 6C and D). I found that viral infectivity was almost undetectable in naive and control vector-transduced Jurkat T cells but the expression of wild-type FcγRIIa significantly enhanced the infectivity of VSV-EBOV GP and EBOV in the presence of ZGP12/1.1, though not CTR IgG. Interestingly, the infection rate of FcγRIIaΔCT-expressing cells was significantly lower than that of cells expressing wild-type FcγRIIa. These results indicated that the FcγRIIa-MAb complex functioned as a receptor-like molecule on this poorly permissive cell line and efficiently promoted infection through the ADE of EBOV entry. More importantly, the results suggested that signaling pathways via the FcγRIIa cytoplasmic tail were likely involved in the ADE of EBOV entry into cells.

Cytoplasmic tail of FcγRIIa is important for enhanced viral uptake. FcγRIIa is known to modulate phagocytosis/macropinocytosis through signaling pathways via its cytoplasmic tail [82,83]. Therefore, to analyze viral binding and intracellular uptake in more detail, I produced DiI-labeled VLPs consisting of the major EBOV structural proteins,

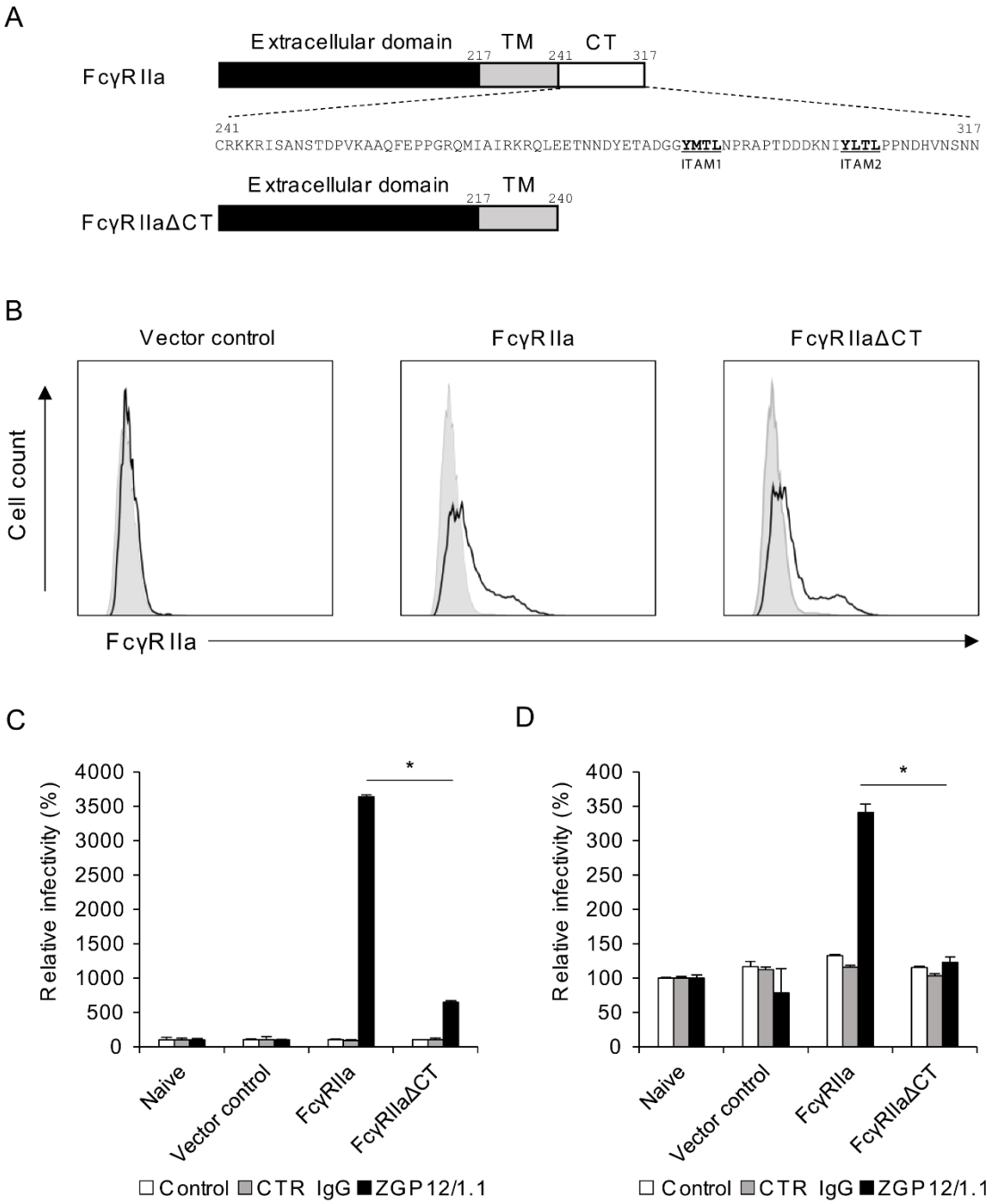

Fig. 6. Importance of FcγRIIa and its cytoplasmic tail in EBOV ADE. (A) Schematic representation of FcγRIIa and FcγRIIaΔCT. TM, transmembrane region; CT, cytoplasmic tail. (B) Cell surface expression of the FcγRIIa ectodomain on Jurkat T cell lines. Jurkat T cells stably expressing FcγRIIa and FcγRIIaΔCT were stained with an anti-CD32 antibody and analyzed by flow cytometry. Black lines represent vector-transduced, FcγRIIa-, and FcγRIIaΔCT-expressing cells. Gray shading represents naive Jurkat T cells. (C and D) Infectivity of VSV-EBOV GP and EBOV in Jurkat T cell lines. VSV-EBOV

GP (C) and EBOV (D) were incubated with medium alone (Control), CTR IgG, or ZGP12/1.1, followed by inoculation into each Jurkat T cell line. At 24 h (C) and 72 h (D) after inoculation, GFP-positive cells were counted. The relative percentage of infectivity in each cell line was calculated by setting the IU value of untreated (Control), CTR IgG-, and ZGP12/1.1-treated viruses in naive Jurkat T cells to 100%, respectively. The mean and standard deviation of three independent experiments are shown. Statistical analysis was performed using Student's *t*-test (*$p<0.05$).

GP, VP40, and NP, and monitored the localization of VLPs in each transduced Jurkat T cell line (Fig. 7). The number of VLPs attached to the surface of naive and empty vector-transduced Jurkat T cells was not significantly different irrespective of the presence of CTR IgG and ZGP12/1.1 (Fig. 7A and C). In contrast, the attachment of VLP was significantly enhanced to similar extents in Jurkat T cells expressing FcγRIIa and FcγRIIaΔCT in the presence of ZGP12/1.1 but not CTR IgG (Fig. 7A and C), suggesting that the FcγRIIa ectodomain expressed on Jurkat T cells had the ability to increase the VLP attachment mediated by ZGP12/1.1. Next, I assessed the number of VLPs incorporated into intracellular vesicles along with Alexa Fluor 647-labeled dextran Mw 10,000 (Alexa647-labeled Dx10), a specific probe for visualizing phagocytotic and macropinocytotic vesicles [11,84]. After incubation for 2 h, ZGP12/1.1-treated VLPs efficiently colocalized with Dx10 in Jurkat T cells expressing wild-type FcγRIIa, but not in cells expressing FcγRIIaΔCT (Fig. 7B and D). Viral uptake was not observed drastically in the absence of FcγRIIa and ZGP12/1.1. Furthermore, the number and size of Dx10-positive vesicles incorporated into Jurkat T cells expressing FcγRIIaΔCT were significantly smaller than those in cells expressing FcγRIIa, indicating the importance of the FcγRIIa cytoplasmic tail in activating the phagocytosis/macropinocytosis (Fig. 7B and E). These data suggested that the ADE infection of FcγRIIa-expressing Jurkat T cells was associated with enhanced viral uptake into cellular vesicles, most likely due to the activation of FcγRIIa-mediated signaling via its cytoplasmic tail.

Intracellular signaling via Src family PTKs contributes to ADE of EBOV infection. To identify the intracellular signaling pathway involved in the ADE of EBOV entry, I analyzed the effects of different inhibitors of signaling pathways in K562 cells, which

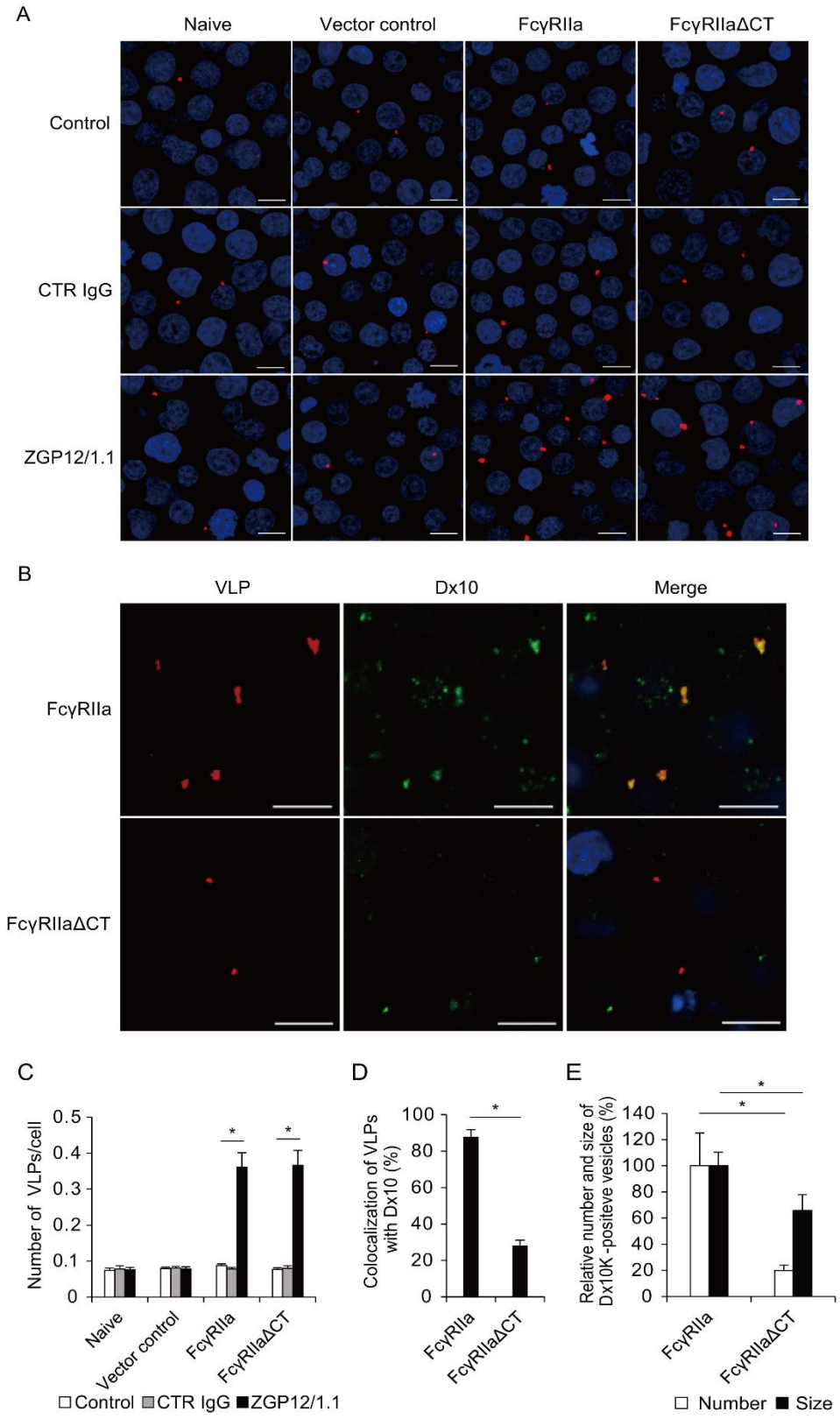

Fig. 7. Importance of FcγRIIa and its cytoplasmic tail in ADE-mediated VLP uptake into cells. (A and B) Fluorescent images of attachment and internalization of VLP. (C-E)

Quantified fluorescent signals of VLP and Dx10. Untreated (Control), CTR IgG-, and ZGP12/1.1-treated DiI-labeled VLPs were inoculated into each Jurkat T cell line and incubated for 30 min on ice. After adsorption, the cells were incubated for 0 h (A and C) or incubated with Alexa647-labeled Dx10 for 2 h at 37 ˚C (B, D, and E). VLPs (red) on the cell surface (A and C) and VLPs (red) and Dx10 (green) in the cytoplasm (B, D, and E) were monitored by confocal laser scanning microscopy. Scale bars represent 10 μm. Nuclei of cells are visualized with DAPI (blue). The number of VLPs attached to the cell surface (C), the colocalization of VLP (DiI) and Dx10 (Alexa647) signals (D), and the number and size of Dx10 (E) were quantified. The number and size were calculated by setting the value of FcγRIIa-expressing Jurkat T cells in the presence of ZGP12/1.1-treated VLPs to 100%. The mean and standard deviation of three independent experiments are shown. Statistical analysis was performed using Student's *t*-test (*$p<0.05$).

naturally express FcγRIIa. Consistent with previous studies [23,77], K562 cells were permissive to VSV-EBOV GP and EBOV infections, and viral infection rates were significantly enhanced in the presence of ZGP12/1.1 (Fig. 8). I then tested inhibitors of Syk and Src family PTK (R788 and PP2, respectively) as these PTKs are known to be principally involved in signaling pathways downstream of FcγRIIa, and in particular to play important roles in inducing FcγR-mediated phagocytosis/micropinocytosis [74,85]. I found that the ADE of VSV-EBOV GP infection was significantly reduced in K562 cells treated with these inhibitors in a dose-dependent manner. In contrast, only a limited reduction was seen in non-ADE infection at the highest concentrations of the inhibitors (Fig. 9). The ADE-specific inhibitory effect was more prominent in cells treated with PP2 than in those treated with R788.

Since Syk is reported to participate in the activation of signaling through PI3K, Btk, and Ras, I further examined which pathways downstream of Syk contributed to the ADE of VSV-EBOV GP infection using specific inhibitors of PI3K (LY294002), Btk (LFM-A13), and Ras (Manumycin A) (Fig. 9). However, both ADE and non-ADE infections by VSV-EBOV GP were dose-dependently reduced by LY294002 and Manumycin A, respectively. LFM-A13 showed little effect on the infectivity of VSV-EBOV GP. Subsequently, I confirmed the effects of these inhibitors using infectious EBOV. Consistent with the data for VSV-EBOV GP, PP2 selectively reduced the ADE, but not the non-ADE infection. Interestingly, R788 showed no effects on the ADE of EBOV infection and rather enhanced the non-ADE infection. LFM-A13 slightly reduced both the ADE and the non-ADE infections, whereas LY294002 and Manumycin A did not inhibit the ADE infection, though Manumycin A slightly inhibited the non-ADE infection.

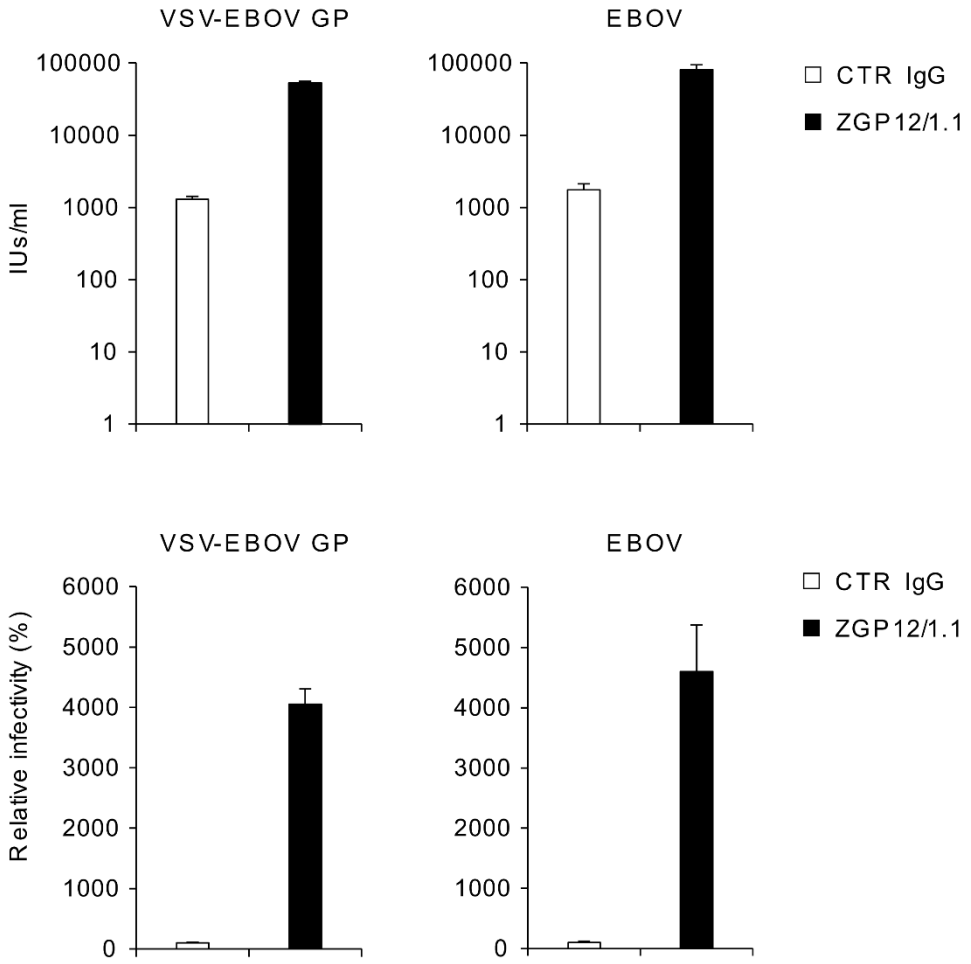

Fig. 8. EBOV ADE in K562 cells. K562 cells were infected with VSV-EBOV GP or EBOV following incubation with CTR IgG or ZGP12/1.1 for 30 min-1 h at 37 ˚C. After incubation for 24 (VSV-EBOV GP) or 72 (EBOV) h, GFP-positive cells were counted and IUs of viruses were determined. The relative percentage of infectivity was calculated by setting the IU value of the viruses in CTR IgG-treated cells to 100%. The mean and standard deviation of three independent experiments are shown.

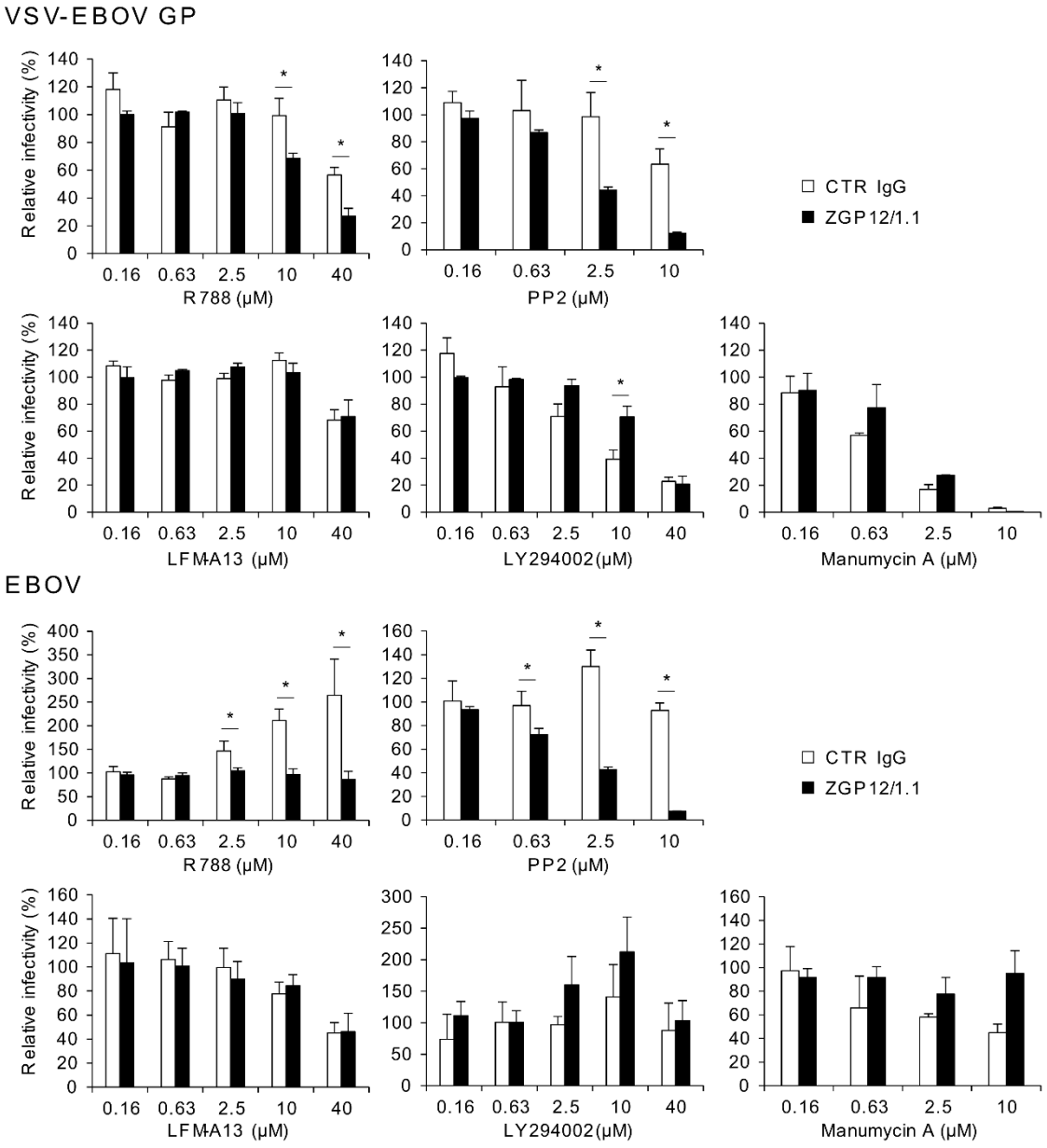

Fig. 9. Identification of FcγRIIa-mediated signaling pathway for EBOV ADE. K562 cells were treated with the indicated concentrations of R788, PP2, LFM-A13, LY294002, or Manumycin A for 1 h at 37 ˚C and inoculated with VSV-EBOV GP or EBOV preincubated with CTR IgG, or ZGP12/1.1. The relative percentage of infectivity was calculated by setting the IU value of the viruses in DMSO or ethanol-treated cells to 100%. The mean and standard deviation of three independent experiments are shown. Statistical analysis was performed using Student's *t*-test (**p*<0.05).

To further investigate the role of Src- and Syk-mediated signaling in EBOV ADE, I generated Src and Syk knockdown K562 cells. K562 cells were transduced with retroviral vectors expressing small hairpin RNAs (shRNAs) for silencing Src or Syk genes (Fig. 10A and B) and infected with VSV-EBOV GP in the presence or absence of ZGP12/1.1 (Fig. 10C). I found that transduced cells stably expressing Src shRNAs (shSrc3 and shSrc4) showed approximately 50% reduction in protein levels (Fig. 10A) and ZGP12/1.1-mediated ADE was significantly decreased in these cell lines (Fig. 10C). In contrast, no significant difference was seen between ADE (ZGP12/1.1) and non-ADE (CTR IgG) infections in Syk knockdown cells although 2 of the Syk shRNAs (shSyk3 and shSyk4) significantly reduced the expression of the Syk protein (Fig. 10B and C).

These results demonstrated that FcγRIIa-mediated signaling through the activation of Src family PTKs contributed to the ADE of EBOV infection, but Syk-related signaling including PI3K, Btk, and Ras did not seem to be specifically involved. I further tested the effect of PP2 in K562/DC-SIGN or K562/hMGL, both of which have been shown to act as attachment receptors for EBOV [77,86], and found that PP2 had limited effects on the infectivity of VSV-EBOV GP in these cell lines (Fig. 11).

VLP-MAb complexes activate phosphorylation of Src in K562 cells. To directly detect the activation of Src family PTKs, I quantified the phosphorylation levels of Src in K562 cells (Fig. 12). I found no significant difference in the cells inoculated with intact VLPs alone at each time point. Likewise, inoculation of CTR IgG-treated VLPs did not enhance Src phosphorylation levels. However, a significant increase of the Src phosphorylation was detected at 30 and 60 min after K562 cells were exposed to ZGP12/1.1-treated VLPs (Fig. 12 left). Furthermore, the enhanced phosphorylation was completely blocked by the

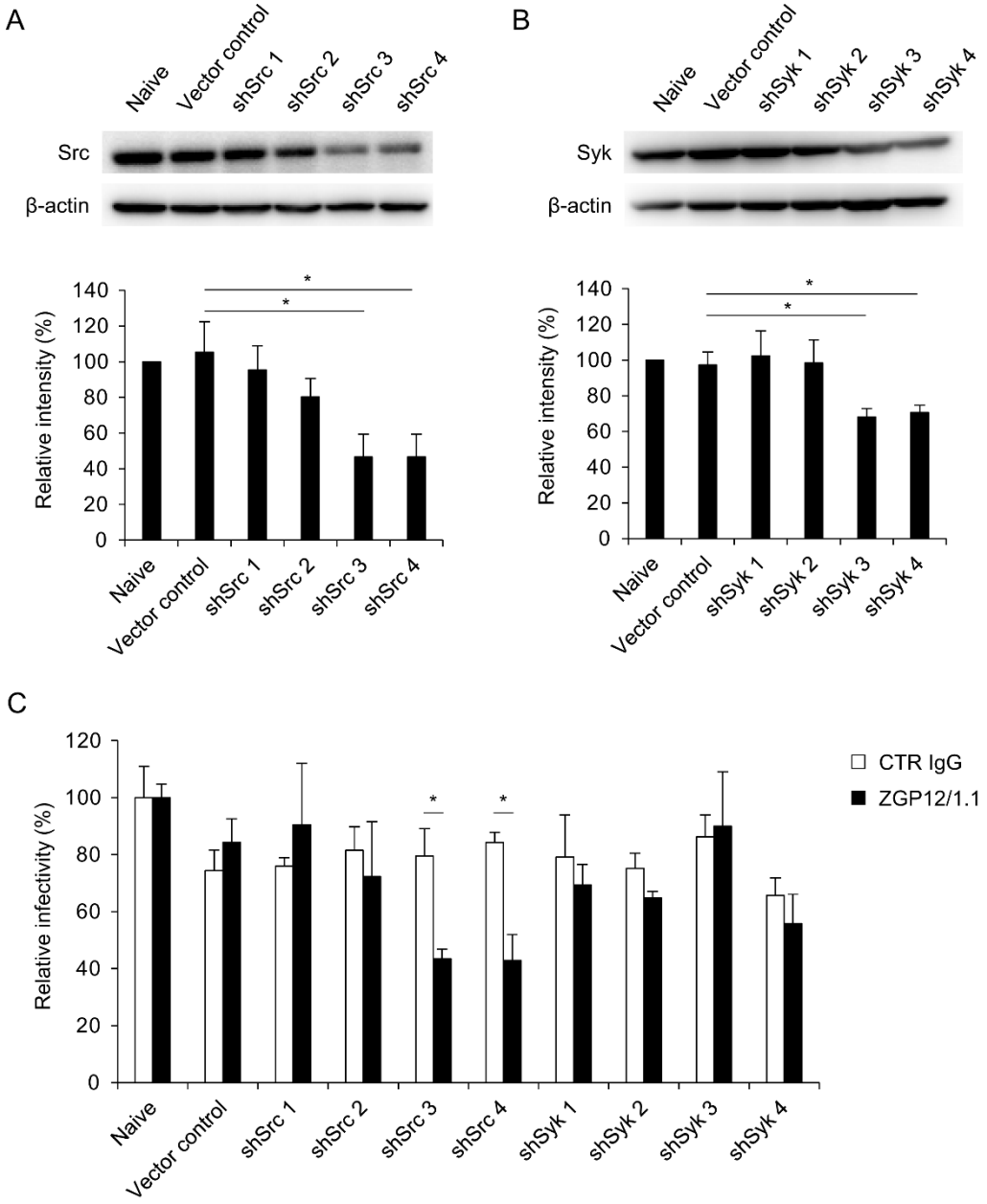

Fig. 10. Effects of Src and Syk knockdown on EBOV ADE. (A and B) Validation of knockdown efficiency of Src and Syk in K562 cell lines. (C) Relative infectivity of VSV-EBOV GP in K562 cell lines. Src (A) and Syk (B) proteins in each cell line were detected by Western blotting. The band intensity of Src and Syk was standardized with that of the β-actin band for each cell line. Relative intensities of the Src and Syk bands were then calculated by setting the intensity of naive K562 cells to 100%. These cell lines were infected with VSV-EBOV GP preincubated with CTR IgG or ZGP12/1.1 (C). The relative percentage of infectivity was calculated by setting the IU value of the viruses in naïve K562 cells to 100%. The mean and standard deviation of three independent experiments are shown. Statistical analysis was performed using Student's *t*-test (*p<0.05).

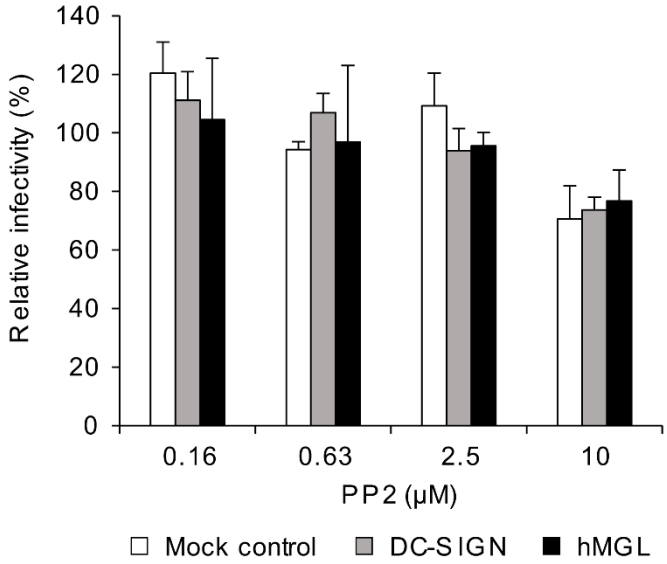

Fig. 11. Effects of PP2 on the VSV-EBOV GP infectivity in K562 cell lines stably expressing C-type lectin. K562/DC-SIGN, K562/hMGL, and mock control K562 cells were treated with DMSO or PP2 for 1 h at 37 ˚C and infected with VSV-EBOV GP in the presence of the inhibitor. After incubation for 24 h, GFP-positive cells were counted. The relative percentage of infectivity was calculated by setting the IU value of the virus in DMSO-treated cells to 100%. The mean and standard deviation of three independent experiments are shown.

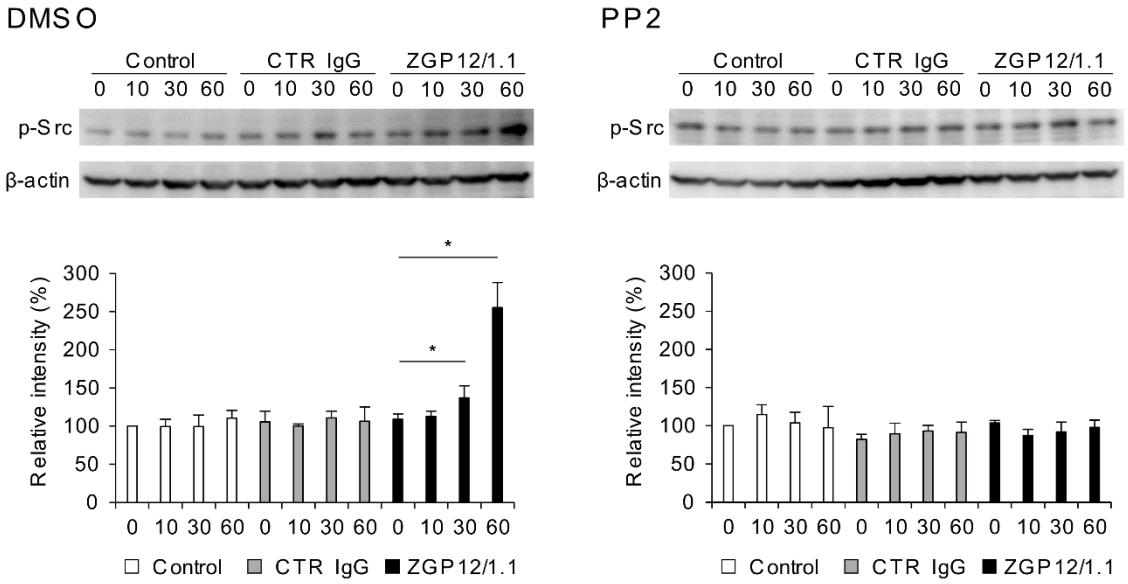

Fig. 12. Increased phosphorylation of Src in K562 cells exposed to the VLP-ZGP12/1.1 complex. Purified VLPs were preincubated with medium alone (Control), CTR IgG, or ZGP12/1.1 and inoculated into K562 cells pretreated with DMSO or PP2 for 1 h at 37 ˚C. At 0, 10, 30, and 60 min post-inoculation, phosphorylation of Src at Tyr416 (p-Src) was detected by Western blotting. The band intensity of p-Src was standardized with that of the β-actin band at each time point. Relative intensities of the p-Src bands were then calculated by setting the intensity of control cells (0 h) to 100%. The mean and standard deviation of three independent experiments are shown. Statistical analysis was performed using Student's *t*-test (**p*<0.05).

Src family PTK inhibitor, PP2 (Fig. 12 right). These findings suggested that Src were activated by the interaction of the VLP-ZGP12/1.1 complex with FcγRIIa.

The ADE of EBOV entry depends on phagocytosis and/or macropinocytosis mediated by Src family PTKs. To further characterize the role of the Src family PTK-dependent signaling in the ADE of EBOV infection, I analyzed the effect of PP2 on the attachment and uptake of DiI-labeled VLPs using K562 cells. I first compared the number of VLPs attached to the cell surface among untreated, CTR IgG-, and ZGP12/1.1-treated VLPs. Since the overexpression of FcγRIIa in Jurkat T cells increased the attachment of VLPs to the cell surface in the presence of ZGP12/1.1 (Fig. 7), I hypothesized that ZGP12/1.1 would enhance the VLP attachment to K562 cells. However, the number of VLPs attached to the cell surface was not significantly different in the presence or absence of ZGP12/1.1 (Fig. 13A left and D), and was not affected by the PP2 treatment (Fig. 13A right and D), indicating that EBOV ADE in K562 cells did not result from increased viral attachment to the cell surface. For the visualization of the VLP uptake into endosomes, K562 cells expressing eGFP-Rab7, a late endosome marker, were used to analyze colocalization of eGFP-Rab7 and internalized VLPs. I found that ZGP12/1.1-treated VLPs were efficiently colocalized with eGFP-Rab7 in K562 cells, whereas only 10-20% colocalization was seen in the cells inoculated with untreated or CTR IgG-treated VLPs (Fig. 13B and E). I further found that the enhanced colocalization of eGFP-Rab7 and ZGP12/1.1-treated VLPs was clearly blocked by the PP2 treatment (Fig. 13C and E). These results indicated that the ADE of EBOV entry into K562 cells was dependent on the Src family PTK activation leading to increased uptake of viral particles into cells.

Finally, I investigated whether the ADE of EBOV entry into K562 cells

depended on phagocytosis/macropinocytosis, which have been shown to be major pathways of the EBOV entry through non-ADE pathways [11-13]. I used Dx10 to visualize phagocytotic and macropinocytotic vesicles in K562 cells and analyzed its colocalization with VLPs. I found that approximately 70% of the ZGP12/1.1-treated VLP signals were overlapped with Dx10 in intracellular vesicles (Fig. 14A and C). Furthermore, the colocalization of Dx10 and ZGP12/1.1-treated VLPs was significantly blocked by the PP2 treatment (Fig. 14B and C). To confirm that these observations were EBOV-specific, I further analyzed DiI-labeled SUDV VLPs and found that ZGP12/1.1 affected neither attachment/uptake of SUDV VLPs nor Dx10 uptake. (Fig. 15). These results suggested that the surface-bound VLP-ZGP12/1.1 complex was incorporated into cells through Src family PTK-dependent phagocytosis and/or macropinocytosis during the ADE of EBOV entry.

A

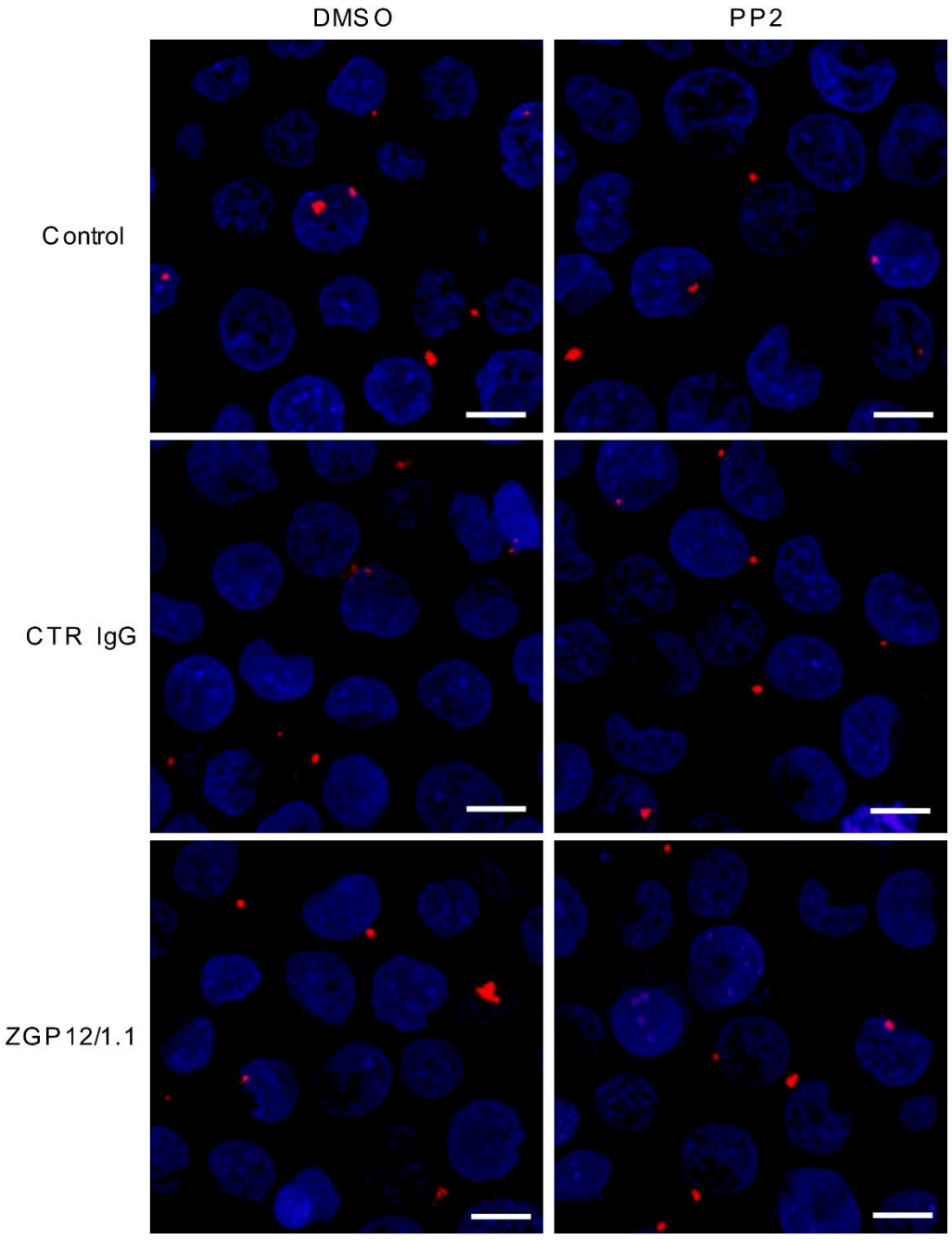

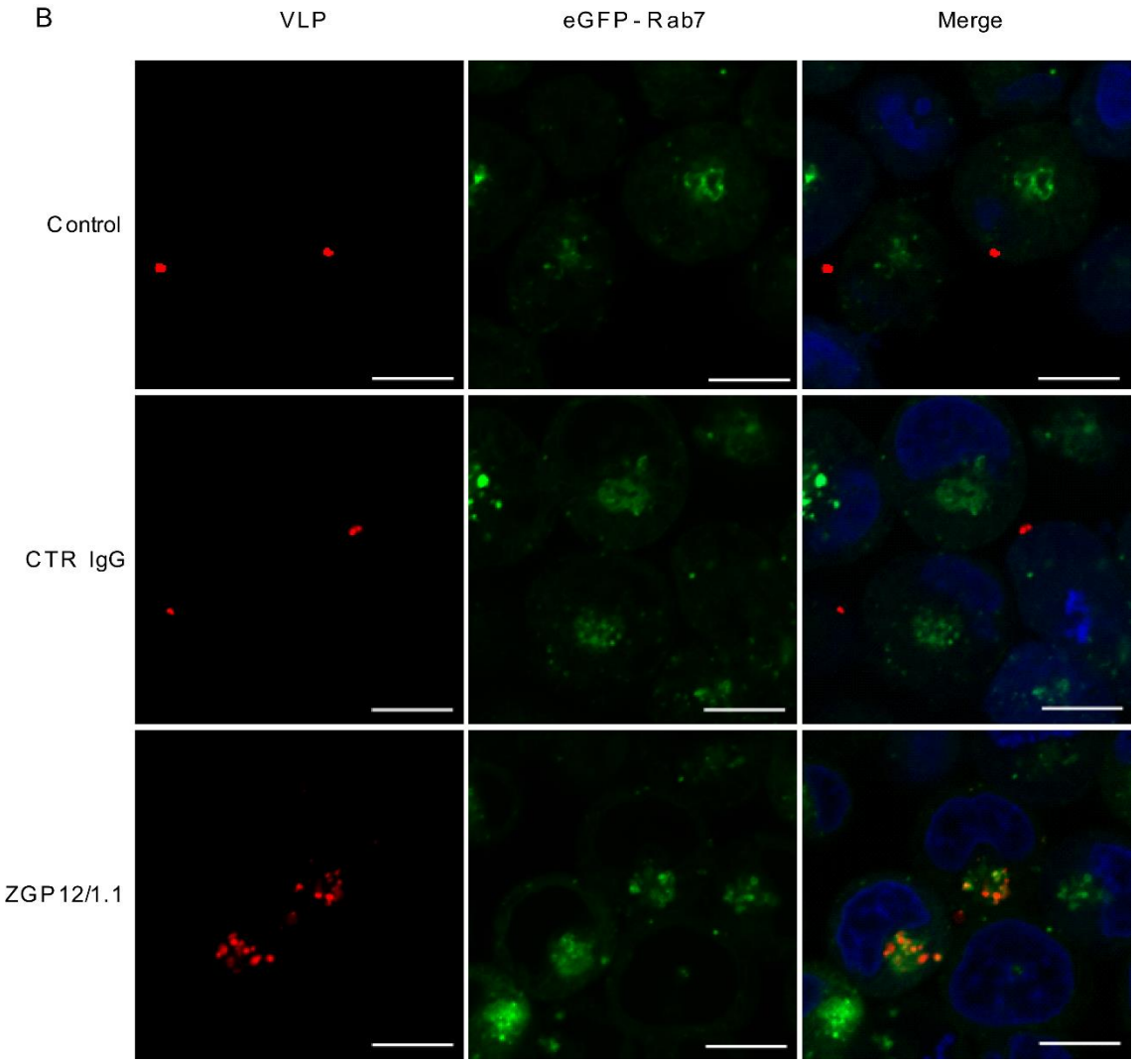
B
VLP
eGFP-Rab7
Merge
Control
CTR IgG
ZGP12/1.1

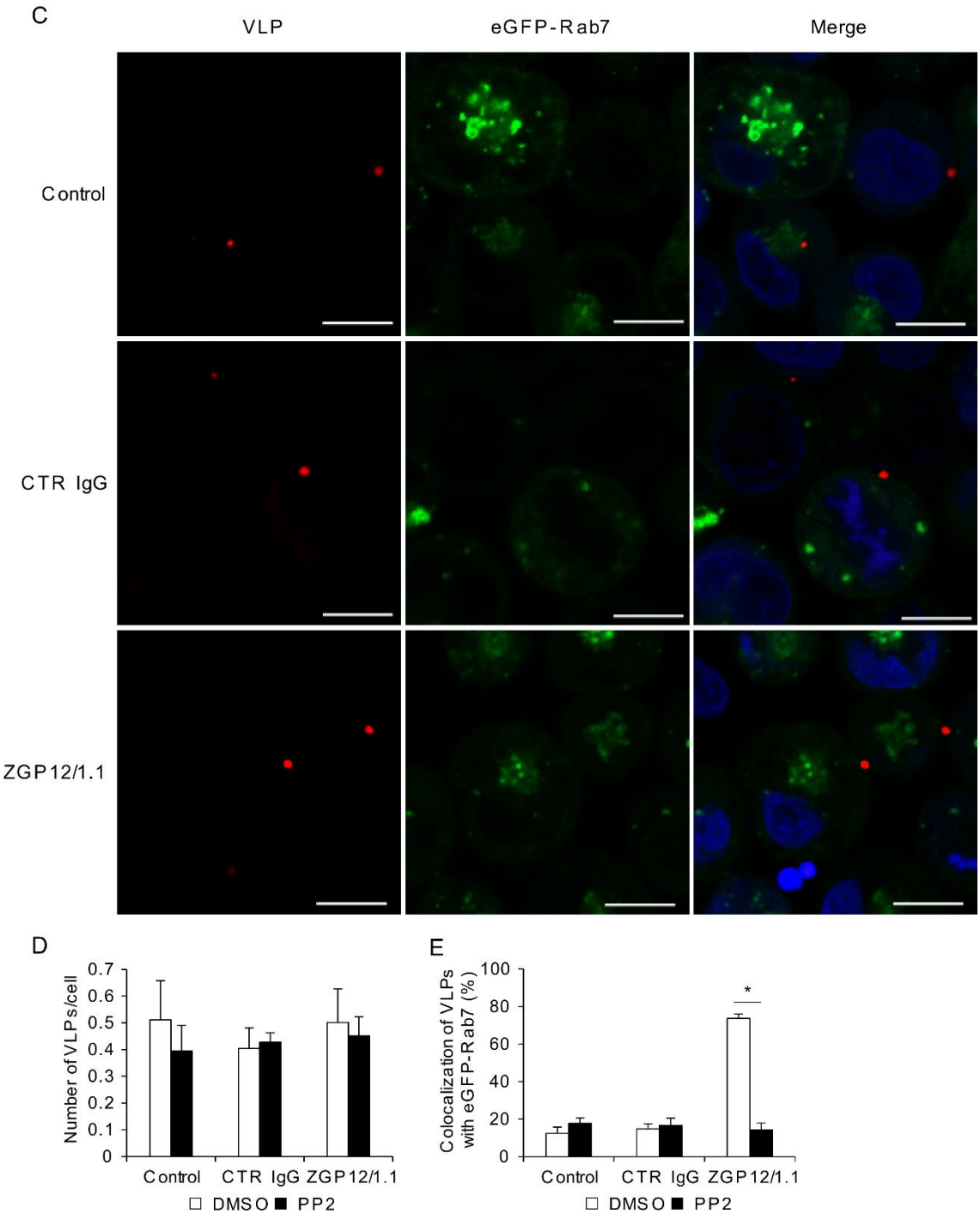

Fig. 13. Enhanced VLP uptake into endosomes in K562 cells during ADE. (A-C) Fluorescent images of attachment and internalization of VLP. (D and E) Quantified fluorescent signals of VLP and Rab7. K562 cells expressing eGFP-Rab7 were incubated with DMSO (A and B) or PP2 (A and C) for 1 h at 37 ˚C. Untreated (Control), CTR IgG-, and ZGP12/1.1-treated DiI-labeled VLPs were inoculated into cells and VLPs (red) on the cell surface at 0 h (A and D) and VLPs (red) and eGFP-Rab7 (green) in the cytoplasm

at 2 h (B, C and E) after adsorption were monitored by confocal laser scanning microscopy. Scale bars represent 10 µm. Nuclei of cells are visualized with DAPI (blue). The number of VLPs on the cell surface (D) and the colocalization of VLPs (DiI) and eGFP-Rab7 signals (E) were quantified. The mean and standard deviation of three independent experiments are shown. Statistical analysis was performed using Student's *t*-test (*p<0.05).

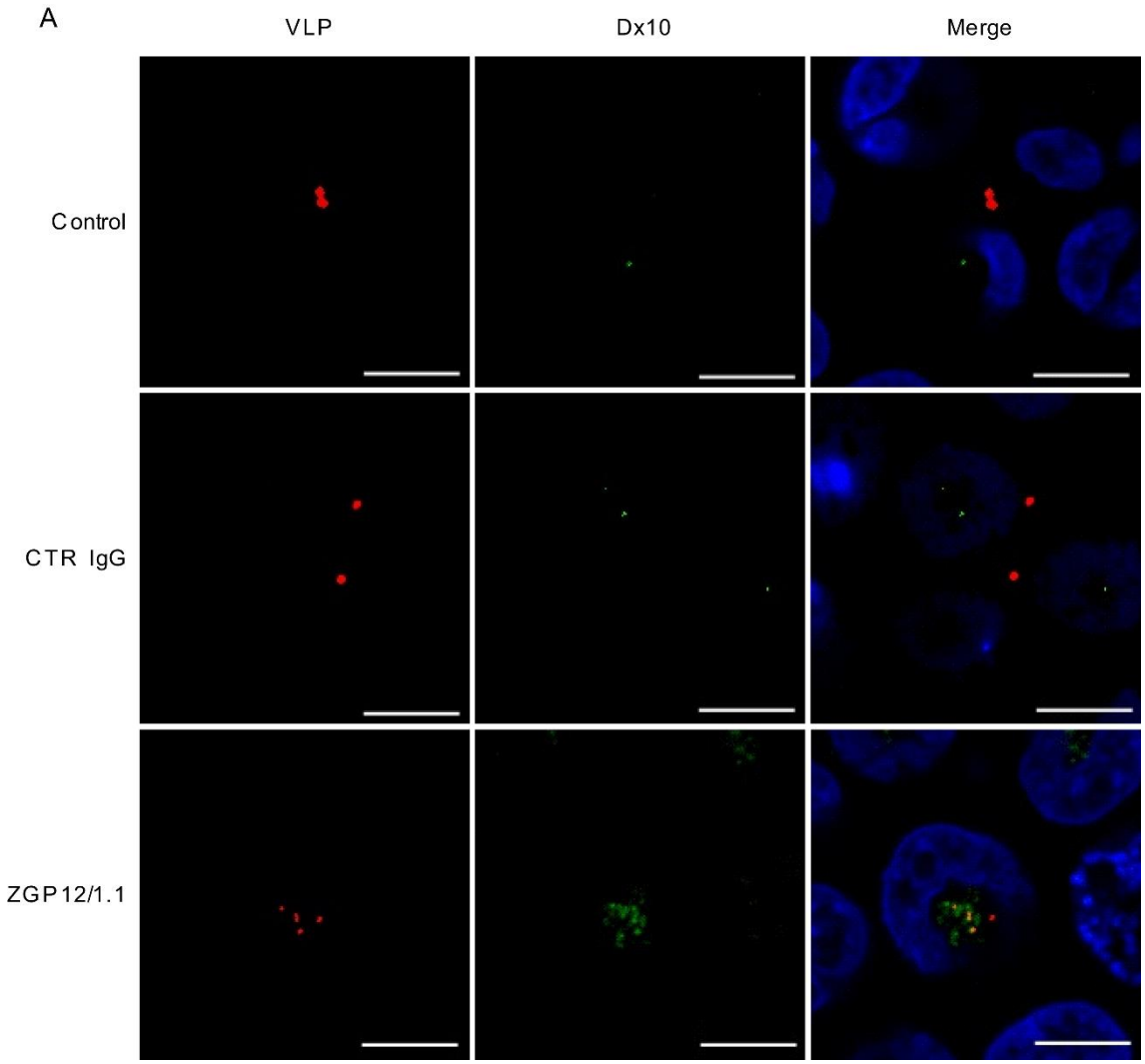
A
VLP
Dx10
Merge
Control
CTR IgG
ZGP12/1.1

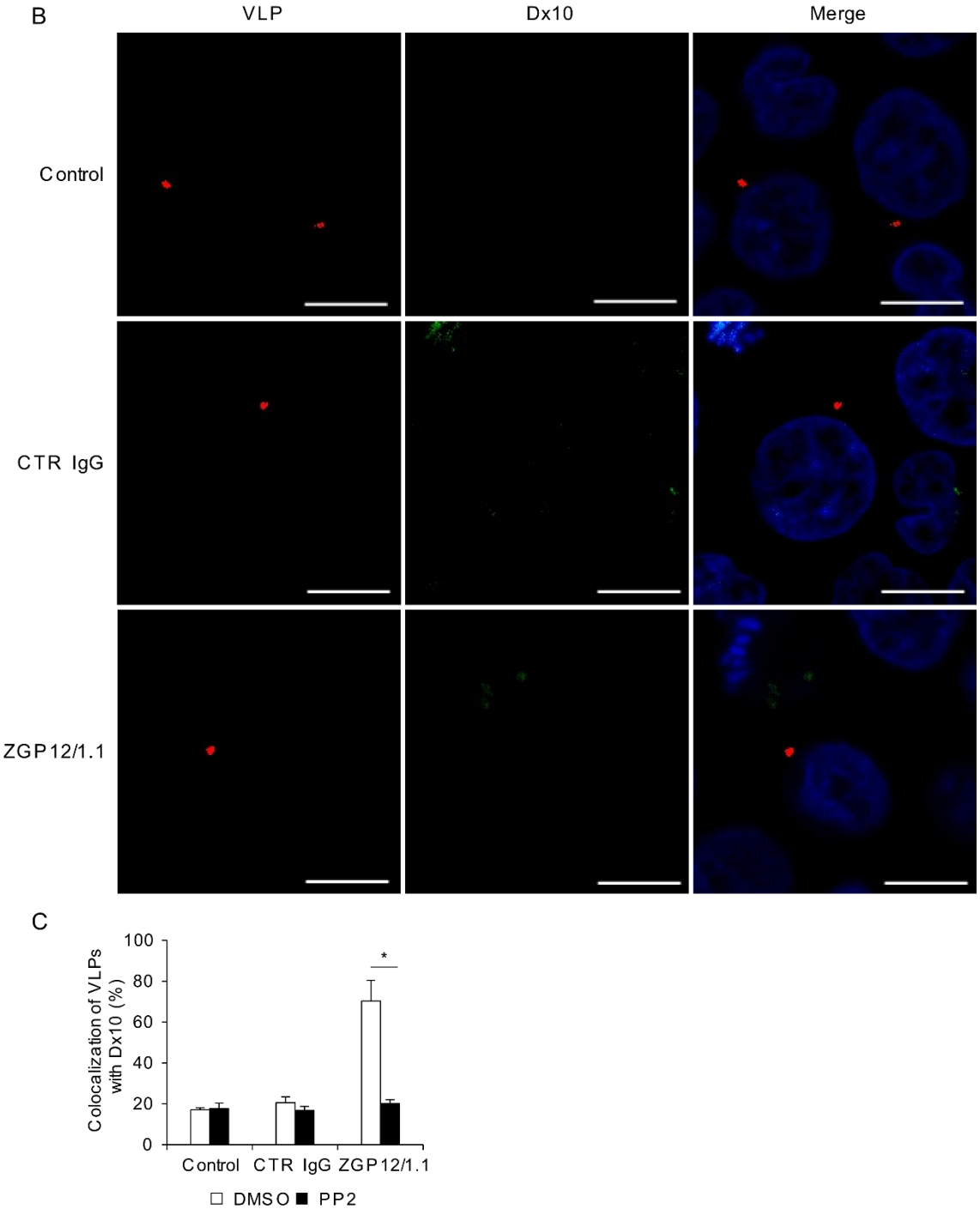

Fig. 14. Colocalization of Dx10 and ZGP12/1.1-treated VLPs. (A and B) Fluorescent images of internalization of VLP and Dx10. (C) Quantified fluorescent signals of VLP and Dx10. K562 cells were incubated with DMSO (A) or PP2 (B) for 1 h at 37 ˚C. Untreated (Control), CTR IgG-, and ZGP12/1.1-treated DiI-labeled VLPs were inoculated into cells and incubated for 30 min on ice. After adsorption, cells were incubated with Alexa647-labeld Dx10 for 1 h at 37 ˚C in the presence of DMSO (A) or

PP2 (B). VLPs (red) and Dx10 (green) in the cytoplasm were monitored by confocal laser scanning microscopy. The colocalization of VLP (DiI) and Dx10 (Alexa647) signals was quantified (C). Scale bars represent 10 µm. Nuclei of cells are visualized with DAPI (blue). The mean and standard deviation of three independent experiments are shown. Statistical analysis was performed using Student's *t*-test (*p<0.05).

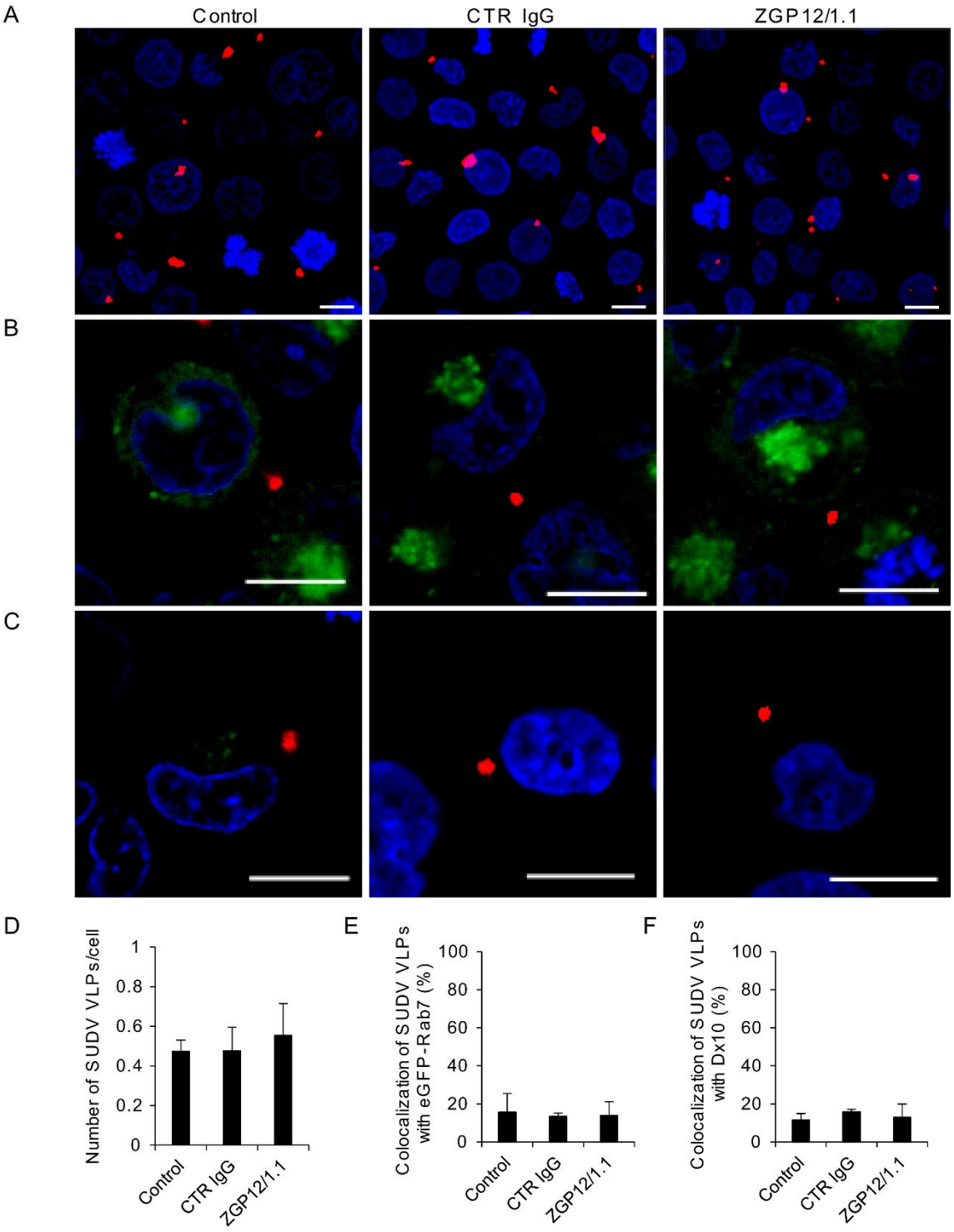

Fig. 15. Attachment, uptake, and localization of DiI-labeled SUDV VLPs. Untreated (Control), CTR IgG-, and ZGP12/1.1-treated DiI-labeled SUDV VLPs were inoculated into K562 cell lines and SUDV VLPs (red) on the cell surface at 0 h (A and D) and VLPs (red) and eGFP-Rab7 (B and E) (green) or Dx10 (C and F) (green) in the cytoplasm at 2 h after adsorption were monitored by confocal laser scanning microscopy. Scale bars

represent 10 μm. Nuclei of cells are visualized with DAPI (blue). The number of SUDV VLPs on the cell surface (D) and the colocalization of SUDV VLPs (DiI) and eGFP-Rab7 (E) or Dx10 (F) signals were quantified. The mean and standard deviation of three independent experiments are shown. Statistical analysis was performed using Student's *t*-test (*p<0.05).

Discussion

It is well established that after the attachment of virus particles to cell surface receptors a variety of signaling pathways are activated through tyrosine and phosphoinositol kinases, and the subsequent cellular events such as endocytosis, including macropinocytosis and phagocytosis, are important for the entry of viruses [87,88]. Likewise, it has been suggested that signaling pathways via FcγR are involved in ADE of virus infections [68]. However, there is limited information on the detailed molecular mechanisms of intracellular signaling pathways required for ADE of virus infection. It has been shown that the non-ADE entry of EBOV requires host factors such as PI3K, the Rho family, and protein kinase C [11,12,89], although the virus-specific receptor molecules involved in these signaling pathways are not yet identified. In the present study, I focused on the ADE of EBOV entry and found that the FcγRIIa-mediated signaling pathway was essential for this process, which is distinct from those required for the non-ADE entry.

The FcγRIIa cytoplasmic tail has been shown to be essential for ADE of dengue virus entry and the involvement of Syk cascade in ADE entry has been reported [90-92]. These data indicate that the cytoplasmic tail of FcγRIIa is crucial for the ADE of EBOV infection and that Src family PTK-dependent signaling is important to enhance viral uptake into cellular vesicles during ADE-mediated entry of EBOV. Src family PTKs are non-receptor tyrosine kinases involved in the regulation of diverse cellular functions like proliferation, differentiation, adhesion, and phagocytosis [93,94]. Importantly, this signaling pathway is known to regulate endocytic machinery by triggering the reorganization of the actin cytoskeleton and membrane remodeling [69,74]. Indeed, previous studies have demonstrated that Src family PTK-dependent signaling is required for the non-ADE entry of some viruses into host cells [95,96]. These data indicate that this signaling is also used to

promote viral particle uptake during the FcγRIIa-mediated ADE of EBOV entry.

It was noted that there was a significant increase (approximately 400%) in infectivity of VSV-EBOV GP when FcγRIIaΔCT is expressed on Jurkat T cells, although it was not as high as wildtype FcγRIIa. This observation suggest that the binding provided by the external portion of FcγRIIa may also have some importance and that the signaling function provided by the cytoplasmic portion of FcγRIIa further enhances the ADE effect. It might also be possible that the FcγRIIa associated with lipid rafts activates some FcγRIIa-mediated signals through its transmembrane domain as described previously [97].

Interestingly, I found that the Syk inhibitor R788 reduced the ADE efficiency of VSV-EBOV GP but not EBOV. While the VSV pseudotype system is widely used to study EBOV GP functions, it has been suggested that pseudotyped VSV and authentic EBOV can utilize different entry pathways since the particle size and structure of pseudotyped VSV do not accurately recapitulate those of EBOV [11,98]. Thus, it may be possible that the EBOV entry primarily relies on macropinocytosis as shown previously [11-13], whereas VSV-EBOV GP can also be incorporated into smaller vesicles. I assume that this difference could influence the effect of the inhibitor since Syk-dependent signaling might be associated with caveolin-mediated endocytosis [99,100]. Another difference found between VSV-EBOV GP and authentic EBOV was that while the Syk inhibitor did not affect EBOV ADE, non-ADE infection was significantly enhanced in the presence of this inhibitor, an effect not observed for VSV-EBOV GP. This might be due to the effect on post-entry mechanisms such as antiviral cellular responses, as proposed by a recent study demonstrating that dengue virus-antibody complexes decreased type-I interferon-stimulated gene expression triggered by the FcγR-mediated signaling pathway through Syk, leading to enhanced replication of the virus [91]. Since such an antiviral response could

be different between VSV- and EBOV-infected cells, it is possible that the Syk inhibitor specifically affected the replication of EBOV, but not VSV, RNA genomes.

Previous studies have demonstrated that cellular C-type lectins such as DC-SIGN and hMGL serve as attachment receptors and promote the entry of EBOV into cells [10,77,86]. These C-type lectins, as well as Fc receptors, are thought to initiate phagocytic pathways for uptake of microorganisms, cell debris, and apoptotic cells [101,102]. Interestingly, both C-type lectins and ADE-antibodies, including ZGP12/1.1, mainly bind to the mucin-like region of EBOV GP, which has a number of N- and O-linked glycosylation sites in the middle portion of the protein [23,77,86], suggesting a similarity in the mechanism of the virus entry mediated by C-type lectins and ADE. However, the Src family PTK inhibitor PP2 showed limited effects on the infectivity of VSV-EBOV GP in the cell lines expressing DC-SIGN or hMGL. Taken together, my data suggest that the FcγRIIa-mediated EBOV ADE principally depends on signaling pathways distinct from those for C-type lectin-mediated entry, while both C-type lectins and ADE-antibody-FcγRIIa complexes are assumed to serve as attachment receptors and subsequent processes for membrane fusion (i.e., cathepsin cleavage and NPC1 binding) appear also to be similar.

In conclusion, these data indicate that EBOV ADE is not simply dependent on increased viral attachment through interaction between FcγRIIa and virus-antibody complexes, and that the induction of FcγRIIa-mediated signaling associated with the activation of Src family PTKs is essential for EBOV ADE. This signaling pathway most likely promotes macropinocytosis, the major entry pathway of EBOV, and leads to enhanced viral uptake into cells. The contribution of Src family PTKs to FcγRIIa-mediated ADE of virus entry has not been demonstrated previously. Discovery of this

ADE mechanism provides a novel perspective for the general understanding of ADE of virus infection. Although the impact of ADE on disease progression remains unclear for many viruses, my findings may offer a potential new target to develop treatments for ADE-associated diseases such as dengue hemorrhagic fever and possibly Zika virus infection [38,103-105], since signaling pathways are known to be essential for virus entry into cells and some signaling inhibitors have been considered to be potential treatment options for virus infections [106-108]. However, since non-ADE entry mechanisms of these viruses are different from EBOV, it is required to investigate whether the Src family PTK-mediated ADE mechanism can be generally applied for other viruses known to utilize ADE entry into cells.

Summary

ADE of EBOV infection has been demonstrated *in vitro*, raising concerns about the detrimental potential of some anti-EBOV antibodies. ADE has been described for many viruses and mostly depends on the cross-linking of virus-antibody complexes to cell surface Fc receptors, leading to enhanced infection. However, little is known about the molecular mechanisms underlying this phenomenon. Here I show that FcγRIIa-mediated intracellular signaling through Src family PTKs is required for ADE of EBOV infection. I found that deletion of the FcγRIIa cytoplasmic tail abolished EBOV ADE due to decreased virus uptake into cellular endosomes. Furthermore, EBOV ADE, but not non-ADE infection, was significantly reduced by inhibition of the Src family PTK pathway, which was also found to be important to promote phagocytosis/macropinocytosis for viral uptake into endosomes. I further confirmed a significant increase of the Src phosphorylation mediated by ADE. These data suggest that antibody-EBOV complexes bound to the cell surface FcγRIIa activate the Src signaling pathway that leads to enhanced viral entry into cells, providing a novel perspective for the general understanding of ADE of virus infection.

Conclusion

GP-specific neutralizing antibodies are known to play an important role in protection against EBOV infection. However, the existing protective MAbs are ebolavirus species-specific. Furthermore, some GP-specific antibodies increase EBOV infection *in vitro*; indeed, ADE is considered a potential problem for the development of vaccines and antibody therapy for EVD.

Thus, in chapter I, I developed and described MAb 6D6 which reduced infectivities of representative isolates of all known ebolavirus species *in vitro*. Antigenic variants escaping from 6D6 had amino acid substitutions within the IFL region which is highly conserved in GPs of all ebolavirus species. MAb 6D6 inhibited the VLP-mediated membrane fusion in endosomes, but did not affect the attachment and internalization of VLPs. Furthermore, passive immunization with 6D6 showed protective effects against EBOV and SUDV in mouse models. The discovery of this cross-neutralizing antibody provides a promising option for broad-acting ebolavirus antibody therapy.

In chapter II, I demonstrated that FcγRIIa-mediated intracellular signaling is a key factor for ADE of EBOV infection. The antibody-virus complex bound to the cell surface FcγRIIa triggered the phosphorylation of Src family PTK that activated signaling pathways leading to enhanced viral uptake into cells through phagocytosis and/or macropinocytosis. These findings provide new insights into the mechanism of ADE-mediated viral infections.

The present study provides important information useful for the design and implementation of improved therapeutics and vaccines whose antiviral effects depend on neutralizing antibodies. Furthermore, since for some viruses ADE has become a great concern to disease control by vaccination and passive immunization, this study

demonstrates the novel perspective for the general understanding of ADE and it may also offer a potential new cellular target to develop treatments for ADE-associated diseases.

Acknowledgments

I express my deepest gratitude to my supervisor, Prof. Ayato Takada (Division of Global Epidemiology, Research Center for Zoonosis Control, Hokkaido Univ., Sapporo, Japan), whose comments and suggestions were innumerably valuable throughout the course of my study. He also provided many opportunities for me to conduct field work abroad and participate in conferences.

I sincerely appreciate the invaluable support and advice provided by Prof. Hirofumi Sawa (Division of Molecular Pathobiology, Research Center for Zoonosis Control, Hokkaido Univ.), Prof. Hideaki Higashi (Division of Infection and Immunity, Research Center for Zoonosis Control, Hokkaido Univ.), and Associate Prof. Kentaro Yoshii (Laboratory of Public Health, Graduate School of Veterinary Medicine, Hokkaido Univ.) during my research work.

I am deeply grateful to Associate Prof. Manabu Igarashi, Specially Appointed Assistant Prof. Reiko Yoshida, and Specially Appointed Assistant Prof. Rashid Manzoor (Division of Global Epidemiology, Research Center for Zoonosis Control, Hokkaido Univ.) for their technical and intellectual support.

I particularly thank Dr. Andrea Marzi, Dr. Heinz Feldmann, Ms. Key Menk, Dr. Atsushi Okumura, Dr. Hideki Ebihara, Dr. Satoko Yamaoka (National Institute of Allergy and Infectious Diseases, National Institutes of Health, Rocky Mountain Laboratories), Dr. Yoshimi Tsuda (Department of Microbiology, Graduate School of Medicine, Hokkaido Univ.), and all the employees at Rocky Mountain Laboratories for their thoughtful advice and cooperation. Working with them proved to be a truly valuable experience.

I am grateful to the coordinator of the Program for Leading Graduate Schools, Hokkaido Univ., Prof. Motohiro Horiuchi (Laboratory of Veterinary Hygiene, Graduate

School of Veterinary Medicine, Hokkaido Univ.), and the members of the Leading Program Office for their help with my PhD coursework.

I thank Dr. Masahiro Kajihara, Dr. Mieko Muramatsu, Dr. Osamu Noyori, Dr. Makoto Kuroda, Dr. Junki Maruyama, Dr. Naganori Nao, and Ms. Hiroko Miyamoto (Division of Global Epidemiology, Research Center for Zoonosis Control, Hokkaido Univ.) for their advice and suggestions. I also thank Mr. Nao Eguchi, Ms. Asako Shigeno, Mr. Tatsunari Kondoh, Mr. Masahiro Sato, and Mr. Yoshihiro Takadate (Division of Global Epidemiology, Research Center for Zoonosis Control, Hokkaido Univ.) for their daily supports.

I wish to specially thank my friends, Ms. Minori Kuroda, Ms. Chiho Kaneko, Ms. Reiko Akamatsu, Ms. Memi Muto, and Ms. Kanae Shiokawa, for their encouragement and time. Finally, I express my gratitude to my family and my husband for their understanding and wonderful support.

My research was funded by the Research Fellowship for Young Scientists from the Japan Society for the Promotion of Science.

和文要旨

エボラウイルスは、フィロウイルス科に属し、ヒトを含む霊長動物に重篤な出血熱を引き起こす病原体である。フィロウイルス科には、進化系統学的にエボラウイルス属、マールブルグウイルス属、およびキュエヴァウイルス属に分類される。マールブルグウイルス属およびキュエヴァウイルス属にはそれぞれ 1 種のみが知られているのに対し、エボラウイルス属は 5 種(*Zaire ebolavirus*、*Sudan ebolavirus*、*Taï Forest ebolavirus*、*Bundibugyo ebolavirus* および *Reston ebolavirus*)に分けられている。2000 年以降、*Zaire ebolavirus*、*Sudan ebolavirus* および *Bundibugyo ebolavirus* によるエボラウイルス病(EVD)がアフリカで頻繁に発生している。これらのウイルスは抗原的に大きく異なっており、属間あるいは種間で交差反応する免疫応答の誘導が困難なため、エボラウイルスに対する予防・治療・診断法の開発にとって問題となっている。2014 年の西アフリカでの *Zaire ebolavirus* による EVD 流行の際には、未承認薬ながら抗体療法が実施されたが、使用されたモノクローナル抗体は *Zaire ebolavirus* による EVD に対してのみ有効である。

第 1 章では、まず、*Zaire ebolavirus* および *Sudan ebolavirus* のウイルス様粒子(VLP)で免疫した BALB/c マウスの脾臓を用いて、5 種のエボラウイルス全てを中和する抗体の作出を試みた。フィロウイルスの表面糖蛋白(GP)を纏った非増殖性シュードタイプ水胞性口炎ウイルス(VSV)に対する中和活性を指標に、抗体産生ハイブリドーマ培養上清をスクリーニングした結果、全てのエボラウイルス種に対して高い中和活性を示すモノクローナル抗体(6D6)が得られた。次に、6D6 存在下で、*Zaire ebolavirus* の GP 遺伝子をもつ増殖性シュードタイプ VSV を培養することによってエスケープミュータントを選択し、GP のアミノ酸配列を親株と比較したところ、エスケープミュータントの GP には、全てのエボ

ラウイルス種において高度に保存されている Internal fusion loop(IFL)のアミノ酸配列内に変異が見られたことから、この領域がエピトープであると推察された。共焦点顕微鏡を用いて蛍光(DiI)ラベルした VLP の細胞への吸着・取込み・膜融合を抗体存在下および非存在下で比較した結果、6D6 はウイルスの細胞侵入過程における膜融合を阻害することが判明した。さらに、6D6 を治療的に投与したマウスは *Zaire ebolavirus* の致死的感染に対し 100%が生残した。また、*Sudan ebolavirus* を感染させたマウスにおいても、6D6 の投与による治療効果が認められた。これらの結果によって 6D6 の投与が複数のエボラウイルスに対して効果的であることが判明した。

一方で、エボラウイルスの GP に対して誘導される抗体の一部は、*in vitro* でウイルスの感染を増強することが知られている(抗体依存性感染増強現象：ADE)。エボラウイルス感染におけるこの現象は、GP に対する抗体が Fcγ 受容体 IIa(FcγRIIa)あるいは C1q と C1q 受容体を介して細胞とウイルスとを架橋することによって引き起こされると考えられているが、ADE の詳細なメカニズムは明らかとなっていない。第 2 章では、FcγRIIa を介する ADE に着目し、FcγRIIa 下流のシグナルと ADE との関連について検討した。まず、エボラウイルス非感受性細胞(Jurkat 細胞)を用いて、FcγRIIa またはその細胞内領域を欠失させた変異体(FcγRIIaΔCT)を強制発現させた細胞を作出し、ADE による感染効率を比較した。その結果、FcγRIIa の細胞内領域が ADE に重要であることが判明した。次に、FcγRIIa を恒常的に発現している K562 細胞を用いて、FcγRIIa 下流の各種シグナル阻害剤の効果を調べ ADE に必要なシグナルの特定を試みたところ、Src family PTK 特異的阻害剤である PP2 が、細胞内の Src family PTK のリン酸化を阻害することによって ADE を介した感染のみを顕著に阻害することが判明した。最後に、共焦点顕微鏡を用いて DiI ラベルした *Zaire ebolavirus* の VLP の細胞への吸

着・取込みを抗体存在下および非存在下で比較した結果、ADE 抗体存在下で、VLP の細胞への吸着数に変化は見られなかったが、細胞内への取り込み効率は上昇していた。さらに、その上昇は PP2 によって阻害された。また、細胞内に取り込まれた VLP はマクロピノサイトーシス/ファゴサイトーシスマーカーとエンドソームに共局在していた。これらの結果によって、ADE 抗体は FcγRIIa 下流の Src family PTKs を介したシグナル伝達経路を活性化し、マクロピノサイトーシス/ファゴサイトーシスを誘導することによって細胞へのウイルスの取り込み効率を上昇させ、その結果、感染増強が引き起こされていることが明らかとなった。

本研究では、既知の全てのエボラウイルス種に対して交差中和活性をしめすモノクローナル抗体を世界に先駆けて作出した。さらに、そのエピトープを解析するとともに中和メカニズムを明らかにし、汎用性の高い EVD 治療用抗体医薬の開発に繋がる重要な知見を提供した。また、ワクチンや抗体医薬開発にとって問題となる ADE のメカニズムを解析し、Src family PTKs を介したシグナル伝達経路が重要であることを見出した。これらの知見は、今後 EVD の予防・治療法開発に大きく貢献することが期待される。

References

1 Feldmann, H. & Geisbert, T. W. Ebola haemorrhagic fever. *Lancet* **377**, 849-862 (2011).

2 Changula, K., Kajihara, M., Mweene, A. S. & Takada, A. Ebola and Marburg virus diseases in Africa: increased risk of outbreaks in previously unaffected areas? *Microbiol. Immunol.* **58**, 483-491 (2014).

3 Kuhn, J. H. *et al.* Virus nomenclature below the species level: a standardized nomenclature for filovirus strains and variants rescued from cDNA. *Arch. Virol.* **159**, 1229-1237 (2014).

4 Baize, S. *et al.* Emergence of Zaire Ebola virus disease in Guinea. *N. Engl. J. Med.* **371**, 1418-1425 (2014).

5 Jeffers, S. A., Sanders, D. A. & Sanchez, A. Covalent modifications of the Ebola virus glycoprotein. *J. Virol.* **76**, 12463-12472 (2002).

6 Volchkov, V. E., Feldmann, H., Volchkova, V. A. & Klenk, H. D. Processing of the Ebola virus glycoprotein by the proprotein convertase furin. *Proc. Natl. Acad. Sci. U S A* **95**, 5762-5767 (1998).

7 Sanchez, A., Trappier, S. G., Mahy, B. W., Peters, C. J. & Nichol, S. T. The virion glycoproteins of Ebola viruses are encoded in two reading frames and are expressed through transcriptional editing. *Proc. Natl. Acad. Sci. U S A* **93**, 3602-3607 (1996).

8 Weissenhorn, W., Carfí, A., Lee, K.-H., Skehel, J. J. & Wiley, D. C. Crystal structure of the Ebola virus membrane fusion subunit, GP2, from the envelope glycoprotein ectodomain. *Mol. Cell.* **2**, 605-616 (1998).

9 Kondratowicz, A. S. *et al.* T-cell immunoglobulin and mucin domain 1 (TIM-1) is a receptor for Zaire Ebolavirus and Lake Victoria Marburgvirus. *Proc. Natl. Acad. Sci. U S A* **108**, 8426-8431 (2011).

10 Alvarez, C. P. *et al.* C-type lectins DC-SIGN and L-SIGN mediate cellular entry by Ebola virus in cis and in trans. *J. Virol.* **76**, 6841-6844 (2002).

11 Nanbo, A. *et al.* Ebolavirus is internalized into host cells via macropinocytosis in a viral glycoprotein-dependent manner. *PLoS Pathog.* **6**, e1001121 (2010).

12 Saeed, M. F., Kolokoltsov, A. A., Albrecht, T. & Davey, R. A. Cellular entry of Ebola virus involves uptake by a macropinocytosis-like mechanism and subsequent trafficking through early and late endosomes. *PLoS Pathog.* **6**, e1001110 (2010).

13 Aleksandrowicz, P. *et al.* Ebola virus enters host cells by macropinocytosis and clathrin-mediated endocytosis. *J. Infect. Dis.* **204**, S957-S967 (2011).

14 Chandran, K., Sullivan, N. J., Felbor, U., Whelan, S. P. & Cunningham, J. M. Endosomal proteolysis of the Ebola virus glycoprotein is necessary for infection. *Science* **308**, 1643-1645 (2005).

15 Schornberg, K. *et al.* Role of endosomal cathepsins in entry mediated by the Ebola virus glycoprotein. *J. Virol.* **80**, 4174-4178 (2006).

16 Carette, J. E. *et al.* Ebola virus entry requires the cholesterol transporter Niemann-Pick C1. *Nature* **477**, 340-343 (2011).

17 Cote, M. *et al.* Small molecule inhibitors reveal Niemann-Pick C1 is essential for Ebola virus infection. *Nature* **477**, 344-348 (2011).

18 White, J. M. & Schornberg, K. L. A new player in the puzzle of filovirus entry. *Nat. Rev. Microbiol.* **10**, 317-322 (2012).

19 Lee, J. E. & Saphire, E. O. Ebolavirus glycoprotein structure and mechanism of entry. *Future Virol.* **4**, 621-635 (2009).

20 Takada, A. *et al.* Identification of protective epitopes on Ebola virus glycoprotein at the single amino acid level by using recombinant vesicular stomatitis viruses. *J. Virol.* **77**, 1069-1074 (2003).

21 Saphire, E. O. & Aman, M. J. Feverish quest for Ebola immunotherapy: straight or cocktail? *Trends Microbiol.* **24**, 684-686 (2016).

22 Takada, A., Feldmann, H., Ksiazek, T. G. & Kawaoka, Y. Antibody-dependent enhancement of Ebola virus infection. *J. Virol.* **77**, 7539-7544 (2003).

23 Takada, A., Ebihara, H., Feldmann, H., Geisbert, T. W. & Kawaoka, Y. Epitopes required for antibody-dependent enhancement of Ebola virus infection. *J. Infect. Dis.* **196**, S347-S356 (2007).

24 Lee, J. E. & Saphire, E. O. Neutralizing ebolavirus: structural insights into the envelope glycoprotein and antibodies targeted against it. *Curr. Opini. Struct. Biol.* **19**, 408-417 (2009).

25 Shedlock, D. J. *et al.* Antibody-mediated neutralization of Ebola virus can occur by two distinct mechanisms. *Virology* **401**, 228-235 (2010).

26 Qiu, X. *et al.* Reversion of advanced Ebola virus disease in nonhuman primates with ZMapp. *Nature* **514**, 47-53 (2014).

27 Dye, J. M. *et al.* Postexposure antibody prophylaxis protects nonhuman primates from filovirus disease. *Proc. Natl. Acad. Sci. U S A* **109**, 5034-5039 (2012).

28 Marzi, A. *et al.* Protective efficacy of neutralizing monoclonal antibodies in a nonhuman primate model of Ebola hemorrhagic fever. *PLoS ONE* **7**, e36192 (2012).

29 Pettitt, J. *et al.* Therapeutic intervention of Ebola virus infection in rhesus macaques with the MB-003 monoclonal antibody cocktail. *Science Transl. Med.* **5**, 199ra113 (2013).

30 Olinger, G. G., Jr. *et al.* Delayed treatment of Ebola virus infection with plant-derived monoclonal antibodies provides protection in rhesus macaques. *Proc. Natl. Acad. Sci.*

U S A **109**, 18030-18035 (2012).

31 Matsuno, K. & Takada, A. Antibody therapy as a future treatment option for Ebola virus infection. *Future Virol.* **2**, 607-614 (2007).

32 McCarthy, M. US signs contract with ZMapp maker to accelerate development of the Ebola drug. *BMJ* **349** (2014).

33 Lyon, G. M. *et al.* Clinical care of two patients with Ebola virus disease in the united states. *N. Engl. J. Med.* **371**, 2402-2409 (2014).

34 Bishop, B. M. Potential and emerging treatment options for Ebola virus disease. *Ann. Pharmacother.* **49**, 196-206 (2015).

35 Meyers, L., Frawley, T., Goss, S. & Kang, C. Ebola virus outbreak 2014: clinical review for emergency physicians. *Ann. Emerg. Med.* **65**, 101-108 (2015).

36 Takada, A. & Kawaoka, Y. Antibody-dependent enhancement of viral infection: molecular mechanisms and in vivo implications. *Rev. Med. Virol.* **13**, 387-398 (2003).

37 Halstead, S. B. Dengue antibody-dependent enhancement: knowns and unknowns. *Microbiol. Spectr.* **2**, 249-271 (2014).

38 Halstead, S. B. Antibody, macrophages, dengue virus infection, shock, and hemorrhage: a pathogenetic cascade. *Rev. Infect. Dis.* **11**, S830-S839 (1989).

39 Takada, A., Watanabe, S., Okazaki, K., Kida, H. & Kawaoka, Y. Infectivity-enhancing antibodies to Ebola virus glycoprotein. *J. Virol.* **75**, 2324-2330 (2001).

40 García-García, E. & Rosales, C. Signal transduction during Fc receptor-mediated phagocytosis. *J. Leukoc. Biol.* **72**, 1092-1108 (2002).

41 Freeman, S. A. & Grinstein, S. Phagocytosis: receptors, signal integration, and the cytoskeleton. *Immunol. Rev.* **262**, 193-215 (2014).

42 Nakayama, E. *et al.* Enzyme-linked immunosorbent assay for detection of filovirus species-specific antibodies. *Clin. Vaccine Immunol.* **17**, 1723-1728 (2010).

43 Bray, M., Davis, K., Geisbert, T., Schmaljohn, C. & Huggins, J. A mouse model for evaluation of prophylaxis and therapy of Ebola hemorrhagic fever. *J. Infect. Dis.* **178**, 651-661 (1998).

44 Takada, A. *et al.* A system for functional analysis of Ebola virus glycoprotein. *Proc. Natl. Acad. Sci. U S A* **94**, 14764-14769 (1997).

45 Shahhosseini, S. *et al.* Production and characterization of monoclonal antibodies against different epitopes of Ebola virus antigens. *J. Virol. Methods* **143**, 29-37 (2007).

46 Kuroda, M. *et al.* The interaction between TIM-1 and NPC1 is important for the cellular entry of Ebola virus. *J. Virol.* **89**, 6481-6493 (2015).

47 Luthy, R., Bowie, J. U. & Eisenberg, D. Assessment of protein models with three-dimensional profiles. *Nature* **356**, 83-85 (1992).

48 Takada, A., Ebihara, H., Jones, S., Feldmann, H. & Kawaoka, Y. Protective efficacy of neutralizing antibodies against Ebola virus infection. *Vaccine* **25**, 993-999 (2007).

49 Both, L. *et al.* Monoclonal antibodies for prophylactic and therapeutic use against viral infections. *Vaccine* **31**, 1553-1559 (2013).

50 Mupapa, K. *et al.* Treatment of Ebola hemorrhagic fever with blood transfusions from convalescent patients. International scientific and technical committee. *J. Infect. Dis.* **179 Suppl 1**, S18-23 (1999).

51 R&D, W. E. *News on vaccines, therapies, diagnostics* (2015).

52 Qiu, X. *et al.* Successful treatment of ebola virus-infected cynomolgus macaques with monoclonal antibodies. *Sci. Transl. Med.* **4**, 138ra181 (2012).

53 Qiu, X. *et al.* Sustained protection against Ebola virus infection following treatment of infected nonhuman primates with ZMAb. *Sci. Rep.* **3**, 3365 (2013).

54 Hernandez, H. *et al.* Development and characterization of broadly cross-reactive monoclonal antibodies against all known ebolavirus species. *J. Infec. Dis.* **212 Suppl 2**, S410-413 (2015).

55 Oswald, W. B. *et al.* Neutralizing antibody fails to impact the course of Ebola virus infection in monkeys. *PLoS Pathog.* **3**, e9 (2007).

56 Audet, J. *et al.* Molecular characterization of the monoclonal antibodies composing ZMAb: a protective cocktail against Ebola virus. *Sci. Rep.* **4**, 6881 (2014).

57 Davidson, E. *et al.* Mechanism of binding to Ebola virus glycoprotein by the ZMapp, ZMAb, and MB-003 cocktail antibodies. *J. Virol.* **89**, 10982-10992 (2015).

58 Reynard, O. & Volchkov, V. E. Characterization of a novel neutralizing monoclonal antibody against Ebola virus GP. *J. Infect. Dis.* **212 Suppl 2**, S372-378 (2015).

59 Wilson, J. A. *et al.* Epitopes involved in antibody-mediated protection from Ebola virus. *Science* **287**, 1664-1666 (2000).

60 Lee, J. E. *et al.* Structure of the Ebola virus glycoprotein bound to an antibody from a human survivor. *Nature* **454**, 177-182 (2008).

61 Dias, J. M. *et al.* A shared structural solution for neutralizing ebolaviruses. *Nat. Struct. Mol. Biol.* **18**, 1424-1427 (2011).

62 Murin, C. D. *et al.* Structures of protective antibodies reveal sites of vulnerability on Ebola virus. *Proc. Natl. Acad. Sci. U S A* **111**, 17182-17187 (2014).

63 Chen, G. *et al.* Synthetic antibodies with a human framework that protect mice from lethal Sudan ebolavirus challenge. *ACS Chem. Biol.* **9**, 2263-2273 (2014).

64 Pal, P. *et al.* Development of a highly protective combination monoclonal antibody therapy against Chikungunya virus. *PLoS Pathog.* **9**, e1003312 (2013).

65 ter Meulen, J. *et al.* Human monoclonal antibody combination against SARS

coronavirus: synergy and coverage of escape mutants. *PLoS Med.* **3**, e237 (2006).

66 Bakker, A. B. *et al.* Novel human monoclonal antibody combination effectively neutralizing natural rabies virus variants and individual in vitro escape mutants. *J. Virol.* **79**, 9062-9068 (2005).

67 Taylor, A. *et al.* Fc receptors in antibody-dependent enhancement of viral infections. *Immunol. Rev.* **268**, 340-364 (2015).

68 Halstead, S. B., Mahalingam, S., Marovich, M. A., Ubol, S. & Mosser, D. M. Intrinsic antibody-dependent enhancement of microbial infection in macrophages: disease regulation by immune complexes. *Lancet Infect. Dis.* **10**, 712-722 (2010).

69 Nimmerjahn, F. & Ravetch, J. V. Fcγ receptors as regulators of immune responses. *Nat. Rev. Immunol.* **8**, 34-47 (2008).

70 Hamada, F., Aoki, M., Akiyama, T. & Toyoshima, K. Association of immunoglobulin G Fc receptor II with Src-like protein-tyrosine kinase Fgr in neutrophils. *Proc. Natl. Acad. Sci. U S A* **90**, 6305-6309 (1993).

71 Ghazizadeh, S., Bolen, J. B. & Fleit, H. B. Physical and functional association of Src-related protein tyrosine kinases with Fc gamma RII in monocytic THP-1 cells. *J. Biol. Chem.* **269**, 8878-8884 (1994).

72 Kiener, P. A. *et al.* Cross-linking of Fc gamma receptor I (Fc gamma RI) and receptor II (Fc gamma RII) on monocytic cells activates a signal transduction pathway common to both Fc receptors that involves the stimulation of p72 Syk protein tyrosine kinase. *J. Biol. Chem.* **268**, 24442-24448 (1993).

73 Joshi, T., Butchar, J. P. & Tridandapani, S. Fcγ receptor signaling in phagocytes. *Int. J. Hematol.* **84**, 210-216 (2006).

74 May, R. C. & Machesky, L. M. Phagocytosis and the actin cytoskeleton. *J. Cell Sci.* **114**, 1061-1077 (2001).

75 Ebihara, H. *et al.* In vitro and in vivo characterization of recombinant Ebola viruses expressing enhanced green fluorescent protein. *J. Infect. Dis.* **196**, S313-S322 (2007).

76 Matsuno, K. *et al.* Different potential of C-type lectin-mediated entry between Marburg virus strains. *J. Virol.* **84**, 5140-5147 (2010).

77 Takada, A. *et al.* Human macrophage C-type lectin specific for galactose and N-acetylgalactosamine promotes filovirus entry. *J. Virol.* **78**, 2943-2947 (2004).

78 Yoshida, R. *et al.* Cross-protective potential of a novel monoclonal antibody directed against antigenic site B of the hemagglutinin of influenza A viruses. *PLoS Pathog.* **5**, e1000350 (2009).

79 Kennedy, G. & Sugden, B. EBNA-1, a bifunctional transcriptional activator. *Mol. Cell. Biol.* **23**, 6901-6908 (2003).

80 Chan, S. Y., Speck, R. F., Ma, M. C. & Goldsmith, M. A. Distinct mechanisms of entry by envelope glycoproteins of Marburg and Ebola (Zaire) viruses. *J. Virol.* **74**, 4933-4937 (2000).

81 Brooks, D. G., Qiu, W. Q., Luster, A. D. & Ravetch, J. V. Structure and expression of human IgG FcRII(CD32). Functional heterogeneity is encoded by the alternatively spliced products of multiple genes. *J. Exp. Med.* **170**, 1369-1385 (1989).

82 Worth, R. G. *et al.* The cytoplasmic domain of FcγRIIA (CD32) participates in phagolysosome formation. *Blood* **98**, 3429-3434 (2001).

83 Araki, N., Hatae, T., Furukawa, A. & Swanson, J. A. Phosphoinositide-3-kinase-independent contractile activities associated with Fcγ-receptor-mediated phagocytosis and macropinocytosis in macrophages. *J. Cell Sci.* **116**, 247-257 (2003).

84 Worth, R. G., Kim, M.-K., Kindzelskii, A. L., Petty, H. R. & Schreiber, A. D. Signal sequence within FcγRIIA controls calcium wave propagation patterns: apparent role in phagolysosome fusion. *Proc. Natl. Acad. Sci. U S A* **100**, 4533-4538 (2003).

85 Kasahara, K. *et al.* Role of Src-family kinases in formation and trafficking of macropinosomes. *J. Cell. Physiol.* **211**, 220-232 (2007).

86 Simmons, G. *et al.* DC-SIGN and DC-SIGNR bind Ebola glycoproteins and enhance infection of macrophages and endothelial cells. *Virology* **305**, 115-123 (2003).

87 Greber, F. U. Signalling in viral entry. *Cell. Mol. Life Sci.* **59**, 608-626 (2002).

88 Mercer, J. & Helenius, A. Virus entry by macropinocytosis. *Nat. Cell Biol.* **11**, 510-520 (2009).

89 Saeed, M. F., Kolokoltsov, A. A., Freiberg, A. N., Holbrook, M. R. & Davey, R. A. Phosphoinositide-3 kinase-Akt pathway controls cellular entry of Ebola virus. *PLoS Pathog.* **4**, e1000141 (2008).

90 Moi, M. L., Lim, C.-K., Takasaki, T. & Kurane, I. Involvement of the Fcγ receptor IIA cytoplasmic domain in antibody-dependent enhancement of dengue virus infection. *J. Gen. Virol.* **91**, 103-111 (2010).

91 Chan, K. R. *et al.* Leukocyte immunoglobulin-like receptor B1 is critical for antibody-dependent dengue. *Proc. Natl. Acad. Sci. U S A* **111**, 2722-2727 (2014).

92 Callaway, J. B. *et al.* Spleen tyrosine kinase (Syk) mediates IL-1beta induction by primary human monocytes during antibody-enhanced dengue virus infection. *J. Biol. Chem.* **290**, 17306-17320 (2015).

93 Berton, G., Mócsai, A. & Lowell, C. A. Src and Syk kinases: key regulators of phagocytic cell activation. *Trends Immunol.* **26**, 208-214 (2005).

94 Okutani, D., Lodyga, M., Han, B. & Liu, M. Src protein tyrosine kinase family and acute inflammatory responses. *Am. J. Physiol. Lung Cell. Mol. Physiol.* **291**, L129-

L141 (2006).

95 Krishnan, H. H., Sharma-Walia, N., Streblow, D. N., Naranatt, P. P. & Chandran, B. Focal adhesion kinase is critical for entry of Kaposi's sarcoma-associated herpesvirus into target cells. *J. Virol.* **80**, 1167-1180 (2006).

96 Li, H. *et al.* Genome-wide gene expression analysis identifies the proto-oncogene tyrosine-protein kinase Src as a crucial virulence determinant of infectious laryngotracheitis virus in chicken cells. *J. Virol.* **90**, 9-21 (2016).

97 Garcia-Garcia, E., Brown, E. J., Rosales, C. Transmembrane mutations to FcgammaRIIA alter its association with lipid rafts: implications for receptor signaling. *J. Immunol.* **178**, 3048-3058 (2007).

98 Cureton, D. K., Massol, R. H., Whelan, S. P. J. & Kirchhausen, T. The length of vesicular stomatitis virus particles dictates a need for actin assembly during clathrin-dependent endocytosis. *PLoS Pathog.* **6**, e1001127 (2010).

99 Samaj, J. *et al.* Endocytosis, actin cytoskeleton, and signaling. *Plant Physiol.* **135**, 1150-1161 (2004).

100 Utskarpen, A. *et al.* Shiga toxin increases formation of clathrin-coated pits through Syk kinase. *PLoS ONE* **5**, e10944 (2010).

101 Stuart, L. M. & Ezekowitz, R. A. B. Phagocytosis: elegant complexity. *Immunity* **22**, 539-550 (2005).

102 Kerrigan, A. M. & Brown, G. D. C-type lectins and phagocytosis. *Immunobiology* **214**, 562-575 (2009).

103 Dejnirattisai, W. *et al.* Dengue virus sero-cross-reactivity drives antibody-dependent enhancement of infection with zika virus. *Nat. Immunol.* **17**, 1102-1108 (2016).

104 Priyamvada, L. *et al.* Human antibody responses after dengue virus infection are highly cross-reactive to Zika virus. *Proc. Natl. Acad. Sci. U S A* **113**, 7852-7857 (2016).

105 Kawiecki, A. B. & Christofferson, R. C. Zika-induced antibody response enhances dengue serotype 2 replication in vitro. *J. Infect. Dis.* **214**, 1357-1360 (2016).

106 Qatsha, K. A., Rudolph, C., Marme, D., Schachtele, C., May, W. S. Go 6976, a selective inhibitor of protein kinase C, is a potent antagonist of human immunodeficiency virus 1 induction from latent/low-level-producing reservoir cells in vitro. *Proc. Natl. Acad. Sci. U S A* **90**, 4674-4678 (1993).

107 Cooper, L., Longnecker, R. Inhibition of host kinase activity altered by the LMP2A signalosome-a therapeutic target for Epstein-Barr virus latency and associated disease. *Antiviral. Res.* **56**, 219-231 (2002).

108 Planz, O. Development of cellular signaling pathway inhibitors as new antivirals against influenza. *Antiviral. Res.* **98**, 457-468 (2013).